AMDG

The Structure of Testis Angiotensin-Converting Enzyme (tACE-g13) in Complex with the Inhibitor RXPA380

ITAI CHITAPI

A minithesis submitted in partial fulfilment of the requirements for the degree of Master of Science (Structural Biology) at the University of Cape Town

Supervisors

Associate Professors B. T. Sewell and E. D. Sturrock

August 2006

KEYWORDS

Active site
Angiotensin-converting enzyme
Glycosylation mutant
Modelling
RXPA380
S2' sub-site
Selectivity
Structure solution
tACE-g13
Tryptophan

ABSTRACT

The Structure of Testis Angiotensin-Converting Enzyme (tACE-g13) in Complex with the Inhibitor RXPA380

I. Chitapi

M.Sc. minithesis, Department of Molecular & Cell Biology, University of Cape Town

Angiotensin-converting enzyme (ACE), a zinc metalloprotease, is a key regulator of the mammalian renin-angiotensin system (RAS). Primarily, ACE is a dipeptidyl peptidase which cleaves angiotensin I to produce angiotensin II, a potent vasoconstrictor. By the same enzymatic mechanism, ACE also inactivates the vasodilator bradykinin. The main overall effect of these actions is an increase in blood pressure. Several ACE inhibitors have been developed as drugs for the treatment of myocardial infarction, hypertension, kidney failure and heart failure.

There are two major isoforms of ACE, somatic and testis ACE (sACE and tACE, respectively). Somatic ACE consists of a C- and N-domain, while testis ACE is essentially identical to the C-domain. Both forms of ACE are heavily glycosylated, a fact that has complicated the structural determination of the enzyme. Discovery of the two-domain structure of sACE led to the realisation that the two domains had different *in vivo* functions, and that the selective regulation of these domains by drugs might lead to improved efficacy and reduced unwanted effects. The side effects of treatment with ACE inhibitors have included angioedema and cough, and have been attributed to the accumulation of bradykinin.

There is ample evidence to suggest that the selective inhibition of only the C-domain may lead to the desired reduction in blood pressure and leave the N-domain unhindered to continue functioning physiologically (for example, clearing bradykinin).

The three-dimensional structural information on tACE and the N-domain, as well as other ACE homologues, has allowed both insights into and speculation about the differences (putative and observed) between the N- and C-domains. A better understanding of the determinants of domain selectivity is the major goal of this project. The C-domain-selective inhibitor, RXPA380, is one of the most C-domain-selective compounds currently available (K_i (C-domain = 3 nM; *cf* K_i (N-domain) = 10000 nM).

The co-crystallisation of tACE-g13, a fully functional glycosylation mutant of tACE, with RXPA380 has enabled the determination by X-ray crystallography of the structure of the tACE-g13–RXPA380 complex, to a resolution of 2.7 Å. This provides new information on the binding of the carboxybenzyl P2 group. The set of interactions between the S2' residues and the P2' tryptophan side chain appears to be, as predicted, the major determinant of the selectivity of RXPA380, as comparisons with the N-domain suggest. In particular, the interactions of the indole ring with two valine residues, and of the indole nitrogen with a water molecule that also has a hydrogen bond to a glutamic acid appear to be the main stabilising interactions. The *in silico* modelling of the tACE–RXPA380 complex gives an inhibitor conformation that, for the most part, corresponds well to the crystal structure.

The determination of the structure of tACE-g13 complexed with this inhibitor confirms the utility of the glycosylation mutant as a structural tool in drug-binding studies. It also provides important insights into the determinants of selectivity, and thus may aid the design of next-generation inhibitors that are domain-selective, tight-binding and physiologically applicable.

August 2006

DECLARATION

I declare that *The Structure of Testis Angiotensin-Converting Enzyme (tACE-g13) in Complex with the Inhibitor RXPA380* is my own work, that it has not been submitted for any degree or examination in any other university, and that all the sources I have used or quoted have been indicated and acknowledged by complete references.

Itai Chitapi 31 August 2006

Signed:

ACKNOWLEDGEMENTS

1. The Carnegie Corporation of New York, the National Research Foundation, the South African Synchrotron Fund, and the University of Cape Town funded this work. I thank the many people who facilitated the financial support from these institutions
2. The assistance and advice of Dr Hassan Belrhali (BM14-UK, ESRF), and Dr Jodi Shaulsky (Accelrys, Inc.) are deeply appreciated.
3. I am thankful to my fellow scientists who have made this work possible: my supervisors Associate Professors Trevor Sewell and Edward Sturrock; my "co-supervisors" Dr Muhammed Sayed, Dr Aloysius Nchinda, and Jean Watermeyer; the UCT/UWC Structural Biology Group (in particular my fellow dudes Serah Kimani, Samuel Kwofie and Margot Scheffer); the Zinc Metalloprotease Group at UCT; Dr Collet Dandara.
4. I acknowledge and thank my friends: those who have been through living with me (Tinashe Makoni, Jonathan Hughes, William Tsolo, Thamba Tabvuma), and those who have not: Rufaro Dhlembeu, Alice Makoni, Jason Brickhill, Melanie Murcott, James Wambugu, Mweli Ndaba, Seike Garny, Malcolm Cocks.
5. I thank those who have provided me with support, inspiration or encouragement at a point, or from a distance, with or without their knowledge: and whom I do not recall at this moment.
6. My foremost supporters, my parents, Hope and Hilary Chitapi: I would be nowhere without you. I thank and bless you both. I am fortunate to have the smartest, most tolerant and loving siblings in the world. Fungai, Rudo and Simbarashe – let's take over the world together!
7. This is the 4-11: *You are worthy, our Lord and God, to receive honour and glory and power, for You created all things, and by Your will they were created and have their being.*

TABLE OF CONTENTS

1. LITERATURE REVIEW

1.1. General biochemistry & substrates

Angiotensin-converting enzyme (ACE) is a vital catalytic component of the mammalian renin-angiotensin system (RAS), a coordinated hormonal cascade that controls blood pressure, renal function, and fluid and electrolyte homeostasis (Skeggs, Jr. et al., 1956; Erdos & Skidgel, 1987; Ehlers & Riordan, 1989). Briefly, ACE cleaves the oligopeptides angiotensin I (Ang I) and bradykinin (BK) to produce angiotensin II (Ang II, vasoconstrictor) and bradykinin$_{1\text{-}7}$ ($BK_{1\text{-}7}$, inactivated vasodilator) (Fig. 1-2). The inhibition of ACE activity has been known for a long time to result in the alleviation of hypertension (Erdos & Skidgel, 1987). ACE occurs in most tissues, but is primarily found in the vascular tissues of lungs and kidneys (Ehlers & Riordan, 1991; Ehlers et al., 1991b). The role of ACE in the RAS, and the interplay between the local RAS and circulating RAS have been previously reviewed (Campbell, 1987; Dzau, 1988; Danser et al., 1999).

The gene coding for ACE has two promoter sites (Soubrier et al., 1993). ACE is a membrane-anchored zinc metalloprotease with two homologous domains, each containing an active site (Soubrier et al., 1988; Wei et al., 1991). It is a dipeptidyl peptidase, cleaving the penultimate peptide bond from various oligopeptide substrates (or their analogues) and releasing a shortened oligopeptide and a C-terminal dipeptide.

The aim of this review is to describe the basic biochemical and catalytic properties of ACE, evaluate the insights gained from structural studies of ACE and related metalloproteases, and propose a line of investigation that will further the understanding and application of domain-selective ACE inhibitors.

1.1.1. ACE isoforms

The non-vertebrate isoforms of ACE, such as the *Drosophila melanogaster* AnCE, generally lack membrane anchors and are therefore soluble (Coates et al., 2000). There are two major isoforms of mammalian ACE, somatic ACE (sACE) and testis ACE (tACE). Somatic ACE is found primarily on the luminal

surface of vascular endothelial cells, in lung capillary cells, and in the brush border (epithelium) of kidney tubules, while testis ACE is found in male germinal cells (Erdos & Skidgel, 1987; Baudin, 2002) (Fig. 1-1). Both isoforms are expressed from a single ACE gene. Somatic ACE is the full protein with 1306 amino acids (but excluding exon 13), and includes a 29-amino acid N-terminal signal peptide (Soubrier et al., 1988). On the other hand tACE is identical to the C-terminal domain of sACE but for its own 31-amino acid N-terminal signal sequence plus the unique O-glycosylation-rich N-terminal sequence encoded by exon 13 (Baudin, 2002). Somatic ACE is shed by proteolysis from the cell membrane into the bloodstream. Testis ACE is cleaved more efficiently, suggesting some sort of regulatory role for the N-domain (Sadhukhan et al., 1998; Woodman et al., 2000). The cleavage site is located at the R^{627}-S^{628}bond (Ehlers et al., 1996; Woodman et al., 2000), although the identity of the shedding enzyme(s) is unknown.

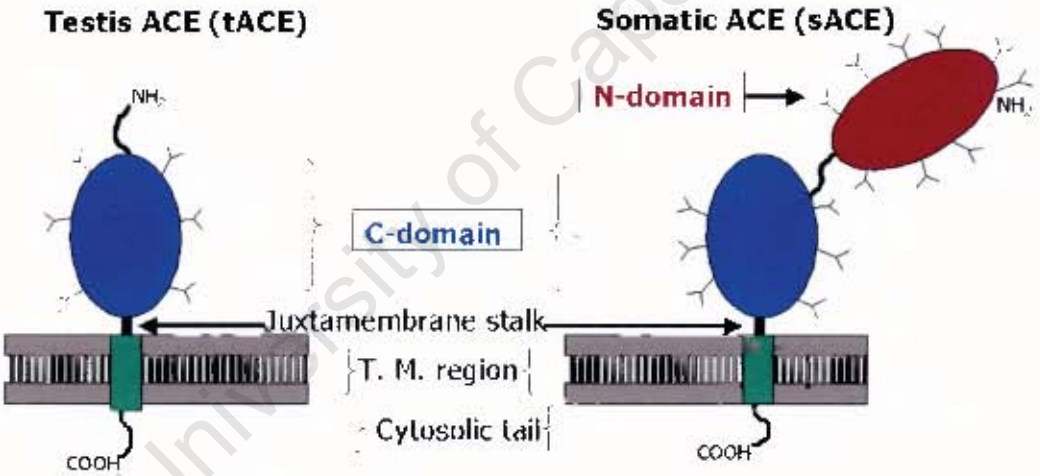

Figure 1-1. Schematic representation of tACE and sACE isoforms. N-linked glycosylation sites are represented by Y-shaped symbols.

Two further forms of human ACE have been isolated: N-domain ACE from ileal fluid (Deddish et al., 1994), and N-domain ACE from the urine of mild hypertensive patients (Casarini et al., 2001). The latter finding, of a 90 kDa form of N-domain ACE, has also been confirmed in spontaneously hypertensive rats, and has been considered for use as a possible genetic marker for hypertension (Bueno et al., 2004). It is proposed that these forms

of ACE are produced by proteolytic cleavage after release of the full length ACE from the membrane (Deddish et al., 1994; Bueno et al., 2004).

Angiotensin-converting enzyme II (ACE2) is a recently discovered carboxypeptidase that removes only the C-terminal residue from Ang I, giving angiotensin$_{1-9}$. It is transcribed from a different gene and has a single catalytic site (Crackower et al , 2002; Oudit et al., 2003)

1.1.2. Glycosylation

ACE is heavily glycosylated, with up to 30% of the molecular weight of tACE being due to N-linked and O-linked glycans (Ehlers et al., 1992). O-glycosylation occurs in the N-terminal region that is unique to tACE, and could play a role in the binding of sperm to oviduct epithelium during the process of fertilisation. However, this region is not critical to its structure or enzymatic function (Ehlers et al., 1992; Kasturi et al., 1994; Baudin et al., 1997).

N-linked glycosylation occurs by means of a highly regulated series of enzymatic reactions. The N-linkage is between the side-chain amide of an asparagine residue and the designated C1 of *N*-acetyl glucosamine, which is in turn typically linked to a series of other glycan residues. This glycosylation can only occur at asparagine (N) residues that are found in the "glycosylation sequon" N-X-S/T, where X is any amino acid except proline (Ronin et al., 1981).

In mammalian cells, highly diverse chains of N-linked glycans may occur, with the result that the surfaces of otherwise identical molecules can be highly heterogeneous. Somatic ACE contains 17 potential N-linked glycosylation sites, 7 of which are in the C-domain. The C-terminal site is not glycosylated, while sites 4-6 are partially (i.e. in some instances) glycosylated, and sites 1-3 are fully (i.e. invariably) glycosylated (Yu et al., 1997) (Fig. 1-1).

A minimal level of glycosylation protects the enzyme from intracellular degradation while targeting it for extracellular secretion, and the unglycosylated enzyme is rapidly degraded (Kasturi et al., 1994; Baudin et al.,

1997). The solubility in extracellular medium may also be dependent on the presence of sufficient glycans on the surface of the enzyme (Baudin et al., 1997). Studies using synthetic membranes have also revealed a likely role of carbohydrates in mediating the dimerisation of ACE (Kost et al., 1998; Kost et al., 2000).

Most critically to structural studies, the glycosylation of ACE has presented a major obstacle in the elucidation of its three-dimensional structure (Gordon et al., 2003; Sturrock et al., 2004). Because glycosylation as a process is not as strictly controlled as code-directed polypeptide synthesis, there is a high degree of oligosaccharide heterogeneity amongst molecules at identical glycosylation sites (Yu et al., 1997). This means that crystallisation, which requires regular packing of identical structures, is very difficult to achieve to the standard required for structural analysis using X-ray crystallography. Two successful approaches to reducing the heterogeneity and aiding crystallisation have been α-glucosidase I inhibition to produce uniform, truncated N-linked glycan chains (Yu et al., 1997), and the mutagenesis of some asparagine residues to glutamine thus preventing N-glycosylation (Gordon et al., 2003). The tACE-lisinopril structure (identical to the C-domain) solved by means of the former approach was the first published structure of any ACE isoform, and revealed that in fact all the putative N-linked glycan chains were at the surface of the enzyme (Natesh et al., 2003). More recently, the structure of the ACE N-domain, expressed in the presence of α-glucosidase I inhibitor *N*-butyldeoxynojirimycin (NBDNJ), has been reported, revealing similar surface glycosylation (Corradi et al., 2006). Watermeyer et al. (2006) have solved the first tACE mutant structure, using a form of tACE (named tACE-g13) in which all but the first and third glycosylation sites have been removed by asparagine-to-glutamine mutagenesis. In addition, the structure of *Drosophila* analogue AnCE (using baculovirus expression in insect cells) has been determined with only two of three possible glycosylation sites intact (Kim et al., 2003), although it is known that AnCE is active even when unglycosylated (Williams et al., 1996). A third approach, the expression of tACE in insect cells using Baculovirus infection (Williams et al., 1994) has also yielded protein that may be amenable to crystallisation for structural studies.

1.1.3. *Chloride activation*

It has long been known that ACE is activated by monovalent anions, in particular chloride, which is the anion typically found associated with ACE under physiological conditions (Bunning & Riordan, 1983). The dependence of ACE on chloride was found to vary with substrate structure, so that, for example, angiotensin I hydrolysis is more dependent on chloride than is bradykinin hydrolysis (Shapiro & Riordan, 1984). It has been suggested that the presence of positively charged residue (K/R) at the C-terminus of a peptide results in greater independence from chloride. Thus, BK_{1-7} accumulates in the absence of chloride, whereas in presence of chloride both BK_{1-7} and BK_{1-5} are produced. The dependence of the two domains on chloride also differs. The C-domain is significantly more dependent on chloride activation than the N-domain (Jaspard et al., 1993). K_i inhibition values for three commercial inhibitors of ACE in differing chloride concentrations (Wei et al., 1992), suggested a chloride-induced conformational change that occurs in the C-domain (and therefore tACE) but not in the N-domain (Natesh et al., 2004). pH is also a determining factor in the chloride activation (Wei et al., 1991; Bersanetti et al., 2004). The 3-dimensional structure of tACE revealed the locations of two chloride ions buried in the interior of ACE (Natesh et al., 2003). Their mechanism of activation of ACE remains elusive, and appears to be indirect as Cl^1 and Cl^2 are 20.7 Å and 10.4 Å from the catalytic zinc, respectively.

1.1.4. *ACE substrates*

In the 1950s, ACE was identified as a factor in horse blood that cleaved angiotensin I to produce the vasoactive angiotensin II (Skeggs, Jr. et al., 1956), and independently as a bradykinin-inactivating enzyme, kininase (Erdos & Yang, 1967) (reviewed by Erdos & Skidgel, (1987)). It has since been found to cleave several other groups of substrates (Sturrock et al., 2004), which will also be described briefly here.

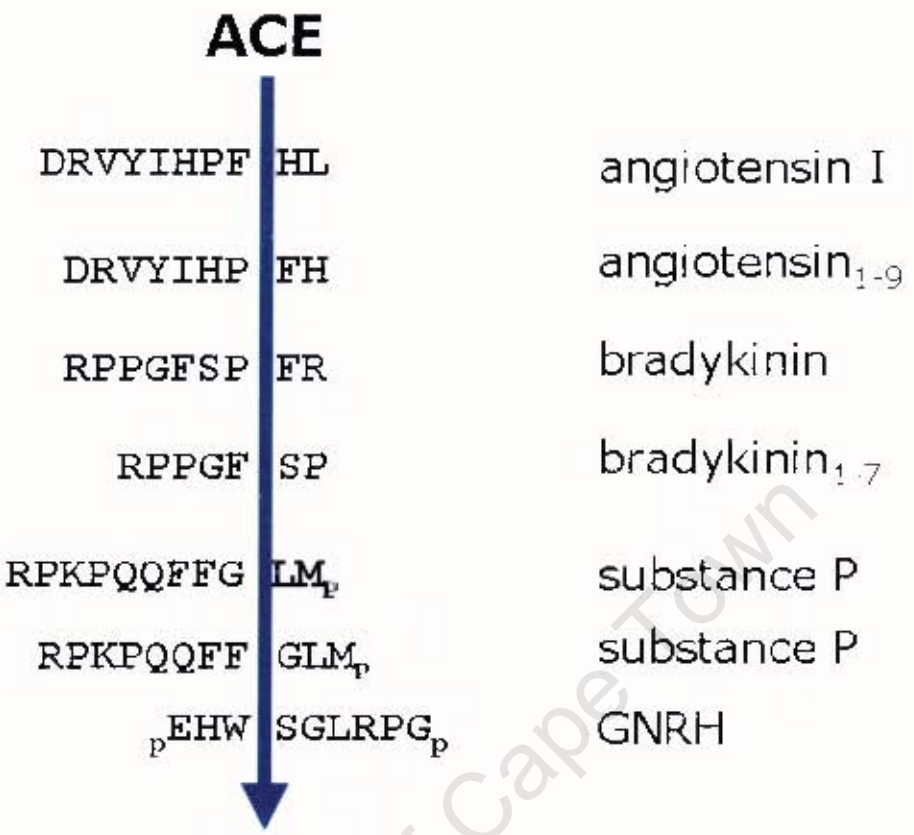

Figure 1-2. Natural ACE substrates and their cleavage sites. $_p$ indicates protection by amidation.

1.1.4.1. Angiotensin

Angiotensin I (a decapeptide, sequence DRVYIHPFHL) is the best-known substrate of ACE. Angiotensin II type I (AT_1) receptors (mainly in heart and vascular smooth muscle cells) are the primary mediators of the vasopressor effects of angiotensin II which result in the upregulation of systemic blood pressure (Eriksson et al., 2002; Turner & Hooper, 2002; Baudin, 2002). Angiotensin II also binds AT_2 receptors, which may counter the effects of AT_1 receptors, and are also considered responsible for cell proliferation, differentiation and angiogenesis (Turner & Hooper, 2002). After the discovery of the two-domain nature of the enzyme (Soubrier et al., 1988; Soubrier et al., 1993), it was observed that both domains catalyse the cleavage of the F-H

peptide bond in angiotensin I, releasing angiotensin II and the C-terminal HL dipeptide. There is an absolute zinc requirement by both domains, as indicated by EDTA inhibition, and affinity (indicated by K_M values) for angiotensin I is similar in both domains (Wei et al., 1991). However there are significant differences in their catalytic rate, chloride activation, and pH dependency (Wei et al., 1991; Wei et al., 1992; Jaspard et al., 1993). Cleavage of angiotensin I is more chloride-dependent than that of bradykinin (Shapiro & Riordan, 1984; Jaspard et al., 1993). Additionally, for angiotensin I hydrolysis, the N-domain is considerably less dependent on chloride activation, whereas the C-domain has an absolute requirement for chloride, and functions optimally at a chloride concentration that is inhibitory to the N-domain (Wei et al., 1991; Jaspard et al., 1993). Taken together, these observations indicate that the C-domain is responsible for most of the *in vitro* hydrolysis of angiotensin I. Experiments using highly selective inhibitors against the C- and N-domains have confirmed that this is also the case *in vivo* (Georgiadis et al., 2003). Interestingly, it was also found that *in vivo* there seems to be a measure of cooperativity between the two domains, since either an N-domain-specific or a C-domain-specific inhibitor reduced Ang I hydrolysis to negligible levels, akin to the effect of double inhibition (Georgiadis et al., 2003). In addition, strong evidence for negative cooperativity between the domains has also been found in bovine somatic ACE, although this was with the artificial substrate FA-Phe-Gly-Gly (Binevski et al., 2003).

1.1.4.2. Bradykinin

Bradykinin (BK) is a nonapeptide (RPPGFSPFR) whose sequential dipeptidyl hydrolysis by ACE leads to the production of two inactivated peptides: BK_{1-7} (RPPGFSP) and BK_{1-5} (RPPGF) (Ehlers & Riordan, 1989). After carboxypeptidase activity has removed the C-terminal arginine, ACE is able to cleave the C-terminal tripeptide (SPF) from the octapeptide, thus performing an endopeptidase function (Erdos & Skidgel, 1987; Baudin, 2002). Jaspard and colleagues (1993) found that both N- and C-domains catalytically cleave BK about 10 times faster than Ang I. This was consistent with prior results of

Bunning and co-workers (1983). As with angiotensin hydrolysis, the C-domain was found to be more chloride-dependent, although the extent of BK-hydrolysis dependence on chloride was less than that of Ang I.

1.1.4.3. N-domain preferred substrates

As soon as the presence of two active sites in ACE was confirmed (Wei et al., 1991), studies were carried out to investigate the differences in their substrate selectivity and catalytic efficiency. There were already hints that differences may exist, based on studies done on well-known substrates as well as artificial substrates of ACE. Gonadotropin-releasing hormone (GnRH, sometimes called Luteinising hormone-releasing hormone (LHRH) in older literature), acts on the pituitary gland to increase the release of gonadotropin and follicle stimulating hormone. GnRH was found to bind sACE somewhat inefficiently (K_M–167 μM) (Skidgel & Erdos, 1985), but the N-domain demonstrated greater catalytic activity with this substrate (Jaspard et al., 1993). ACE releases tripeptides from both the N-terminal and C-terminal ends. It can also sequentially cleave dipeptides from the C-terminus after release of the C-terminal tripeptidyl to produce the N-terminal tripeptide (Skidgel & Erdos, 1985).

N-acetyl-seryl-aspartyl-lysyl-proline (Ac-SDKP) is a natural tetrapeptide involved in the regulation of haematopoietic stem cell proliferation. It inhibits the entry of these pluripotent cells into *S*-phase (DNA replication) and thus restricts proliferation. It may also be an important endogenous negative regulator of fibroblast proliferation in the heart, thus reducing fibrosis and playing a cardioprotective role (Rhaleb et al., 2001). Ac-SDKP is cleaved by ACE at the D-K bond to release Ac-SD and KP. More specifically, it was found that the hydrolysis of Ac-SDKP occurs primarily at the N-domain, which is 50 times more catalytically efficient than the C-domain for the substrate (Rousseau et al., 1995). Captopril is an effective inhibitor of this hydrolysis, both *in vitro* (Rousseau et al., 1995) and *in vivo* (Azizi et al., 1996).

Ang_{1-7} is a product of Ang I metabolism via several different peptidases, such as neprilysin (but excluding ACE) (Ferrario & Iyer, 1998). This peptide has

been found to play a significant role in the regulation of angiotensin metabolism, primarily as it competitively inhibits the somatic ACE C-domain. In addition, Ang_{1-7} is cleaved by the ACE N-domain to give Ang_{1-5} (Deddish et al., 1998).

1.1.4.4. C-domain preferred substrates

Substance P is a neuropeptide with the sequence $RPKPQQFFGLM_n$ (Erdos & Skidgel, 1987). ACE cleaves the C-terminal dipeptide and tripeptide from this undecapeptide, although the physiological significance of this is unclear. The C-domain demonstrates four-fold higher catalysis to the tripeptide against both its production of the dipeptide and the N-domain's production of the tripeptide. The C-terminal methionine residue is said to be protected by amidation (Erdos & Skidgel, 1987). It has been proposed that the presence of an amide group on the C-terminus of Substance P, GnRH and other substrates provides leeway for the peptide substrate to "slip", allowing cleavage of the C-terminal tripeptide rather than or in addition to the dipeptide (Kim et al., 2003).

ACE has also been found to cleave other neuropeptides *in vitro*, such as neurotensin, as well as several enkephalins (Erdos & Skidgel, 1987).

1.1.4.5. Artificial substrates

A number of artificial substrates have been developed for enzymological studies of ACE. These tend to be shorter than natural peptide substrates, and typically contain peptides or peptidomimetic residues linked to a moiety that is detectable by fluorimetric, radiometric, photometric, or other means for enzyme assays (Baudin, 2002). They are often commercially available and easier to acquire than some peptide substrates. These include Z-Phe-His-Leu, hippuryl-histidyl-leucine (HHL), and furylacryloyl-phenylalanyl-glycyl-glycine (FA-Phe-Gly-Gly). The latter two demonstrate the pattern of dependency on chloride shown by Ang I (Baudin, 2002), with an optimal

chloride concentration for HHL hydrolysis by the N- and C-domains of 10 and 800 mM respectively (Wei et al., 1991).

In a fascinating study Araujo and colleagues (2000) used fluorescence resonance energy transfer and several peptide sequences to determine some of the amino acid preferences of the C- or N-domain, particularly at the P1' position. With a similar protocol, Bersanetti et al. (2004) have developed a series of short fluorogenic peptide substrates, one of which (peptide sequence LFK) has shown (~70-fold) selectivity for the C-domain.

1.1.5. Enzyme mechanism

In both the N- and C-domains of ACE, there is a conserved catalytic sequence that is characteristic of the gluzincin family of zinc metalloproteases (Hooper, 1994). The consensus sequence consists of the HEXXH motif, the two histidines of which coordinate the zinc atom, and a glutamic acid, (24 residues downstream), which is the third zinc-coordinating residue.

The mechanism of action of ACE was thought to mimic that of the prototypical zinc metalloprotease thermolysin, whose mechanism of action was elucidated in several studies and summarised by Matthews (Fig. 1-3) (Matthews, 1988). Briefly, the reaction in ACE proceeds as a fairly typical general-base catalysis. A water molecule associated to the zinc attacks the carbonyl carbon of the scissile bond of the substrate. The glutamic acid (E^{384}) of the metalloprotease signature HEXXH motif acts as the acceptor of a proton from the water. The negatively charged oxygen resulting from the binding of OH is stabilised by the zinc, as well as Y^{523} and a water in this intermediate (in thermolysin these correspond to a histidine and tyrosine, respectively). As the reaction proceeds, the E^{384} releases its proton to the amine nitrogen, thus destabilising the scissile bond. This bond's nitrogen atom is stabilised by electrostatic interactions with the backbone carbonyls of A^{354} and S^{355}. The consequent charge repulsion between the new amino terminal and zinc, as well as the stabilisation of the C-terminal by the same, leads to separation of the products.

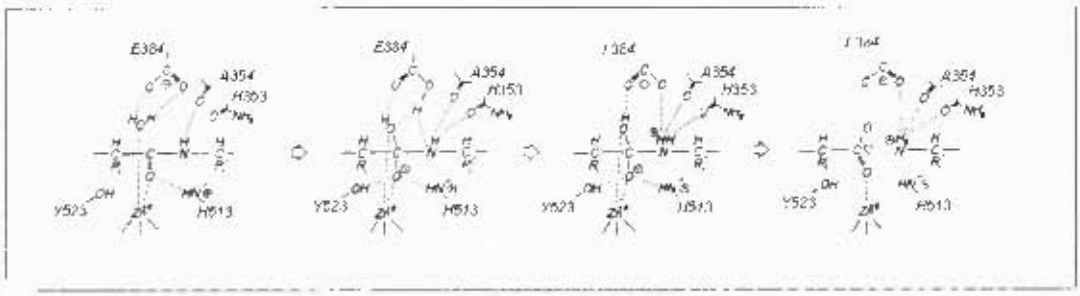

Figure 1-3. Catalytic mechanism of tACE, adapted from Matthews (1988).

1.2. ACE inhibitors

The first ACE inhibitors were discovered as bradykinin-potentiating peptides from the venom of the South American snake *Bothrops jararaca*, as well as other venomous snakes (Cushman et al., 1977; Cushman & Ondetti, 1999). Based on these, a good understanding of the carboxypeptidase A active site, and some modest computer modelling capabilities, Cushman and co-workers developed captopril, which became the first clinically-approved inhibitor of ACE (Cushman et al., 1977; Ondetti et al., 1977). Many different ACE inhibitors have been designed since then – as of 2002 there were seventeen different inhibitors of ACE in clinical use (Zaman et al., 2002). The inhibitors can be categorised into major types determined by the number of amino acid substituent groups. Type I inhibitors have four amino acid (substituent) groups, designated P2, P1 (on the N-terminal side of the zinc-binding group), P1' and P2' (C-terminal groups) (Schechter & Berger, 1967). Type II inhibitors have P1, P1' and P2' groups only, while Type III consist only of the C-terminal P1' and P2' groups and the zinc binding group (Fig. 1-4). An alternative classification promotes the chemical character of the zinc-binding motif as the major criterion for classification. By this means, compounds can be clustered into six classes (Redelinghuys et al., 2005) –

- Sulphydryls – captopril is the prototype member of this group. The inhibitor's coordination with the catalytic zinc atom is via a C-terminal – SH group. These inhibitors are also known as Type III inhibitors, as they only have P1' and P2' substituents.

- Ketones – this group of compounds includes both Type I and Type II molecules. Coordination to the zinc atom is by means of the ketone functional group.

- Carboxylates – as the name suggests, the carboxylate moiety is responsible for binding to zinc. Many of the clinical inhibitors belong to this group, and as they tend to be peptides or peptide analogues they are often delivered to the body as esters to improve bioavailability. This group includes enalapril and lisinopril, two well-established anti-ACE drugs.

- Hydroxamates – Turbanti and coworkers (Turbanti et al., 1993) pioneered the development of Type III inhibitors with a new zinc-binding moiety, the hydroxamic acid functional group. The non-amino acid nature of the compounds and the stereochemistry potential play a role in making the hydroxamates an alternative group of interest.

- Silanediols – these compounds take advantage of the ability of silicon to form a stable dialkylsilanediol (Kim & Sieburth, 2004). Since silicon does not form double bonds except under duress, this form can act as a stable (unhydrolysable) mimic of the tetrahedral intermediate that forms during substrate catalysis. In addition, silanediols are neutral at physiological pH, unlike hydrated carbonyl isosteres (Kim & Sieburth, 2004; Kim et al., 2005)

- Phosphinates – this functional group of compounds has been long known as potent inhibitors of zinc metalloproteases (Yiotakis et al., 1994). Recently domain-selective Type I inhibitors have been developed that show nanomolar inhibition constants selectively for one or other of the domains of ACE (Dive et al., 1999; Junot et al., 2001; Dive et al., 2004; Georgiadis et al., 2004).

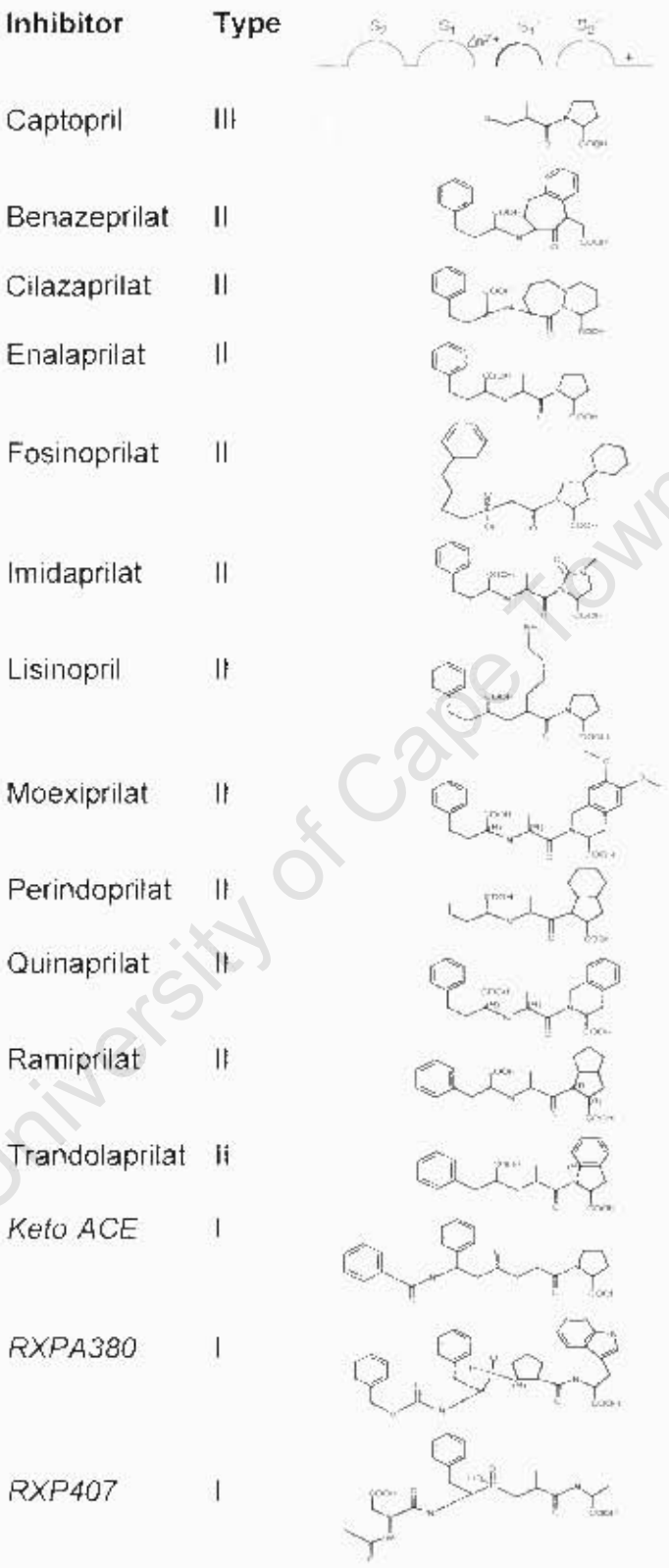

Figure 1-4. Chemical structures and inhibitor types of a range of ACE inhibitors. The inhibitor moieties are positioned so as to indicate the ACE active site sub-site that accommodates them. Inhibitors in *italics* are not in clinical use.

1.3. Three-dimensional structure of Angiotensin-converting enzymes and related metalloproteases

1.3.1. Introduction – metalloproteases

The prototypical metalloproteases for ACE in terms of tertiary structure have been thermolysin and carboxypeptidase A (Colman et al., 1972; Lipscomb, 1983). The structures of these two metalloproteases have both been known for over 20 years, and indeed the active site of carboxypeptidase A was used as a model for ACE in the early days of inhibitor design (Cushman et al., 1977; Ondetti et al., 1977). Structures of other metalloproteases have been elucidated. Both leukotriene 4A hydrolase/aminopeptidase (Thunnissen et al., 2002) and neutral endopeptidase or neprilysin (Oefner et al., 2000) have catalytic sites that are notably similar to that of tACE.

The structure of neurolysin, a representative of the M3 family of metallopeptidases, revealed an elliptical protein containing a narrow channel that limits access to the active site (Brown et al., 2001). This discovery helped to explain the size range restriction of neurolysin substrates. Like ACE, neurolysin is able to hydrolyse a range of substrates, but its major physiological substrate is the important neuropeptide neurotensin ($_{p}$ELYQNKPRRPYIL), from which the C-terminal tripeptide is cleaved. Apart from the zinc-binding motif, there is no significant sequence similarity between neurolysin and ACE; however, the three-dimensional structures of the two metalloproteases are quite similar (Acharya et al., 2003).

The structure of a carboxypeptidase from the extreme thermophile *Pyrococcus furiosus*, was found to bear a striking resemblance to the neurolysin structure, and therefore to tACE (Arndt et al., 2002). This enzyme functions optimally at a temperature between 90°C and 100°C, and more unusual is that it is *inactive* when zinc is bound to the active site, but shows

activity when various other metals, such as cobalt, are bound (Cheng et al., 1999).

It appears that the overall architecture of the zinc metalloproteases allows for a variety of conformations and diverse sequences for differing environments and particular functions, with a premium conservation of the catalytic motif.

1.3.2. ACE structures – C-domain/tACE

Several crystal structures of angiotensin-converting enzyme and its homologues have been solved recently. The following sections describe these crystal structures. All the angiotensin-converting enzyme homologues (truncated to exclude trans-membrane and intracellular domains in the case of tACE and ACE2) have overall elliptical structures. The active site is contained within a cavity or groove at or near the centre of the molecule.

1.3.2.1. Testis ACE (1o8a) and tACE–lisinopril (1o86)

Testis ACE was expressed and crystallised in the presence of an α-glucosidase I inhibitor (Gordon et al., 2003). The three-dimensional structure was determined by X-ray diffraction. The molecule is a predominantly helical structure, with only a few short β-strands interrupting the dominant helices (20 α- and 7 3^{10}-helices) that are separated by short loops (Natesh et al., 2003) (Fig. 1-5, Fig. 1-6). The α-helices 1 and 2 comprise the "top lid" at the N-terminal end of the molecule, preventing access of large substrates to the active site (Fig. 1-6). A central groove extending about 30 Å into the molecule divides it into 2 sub-domains (Natesh et al., 2003).

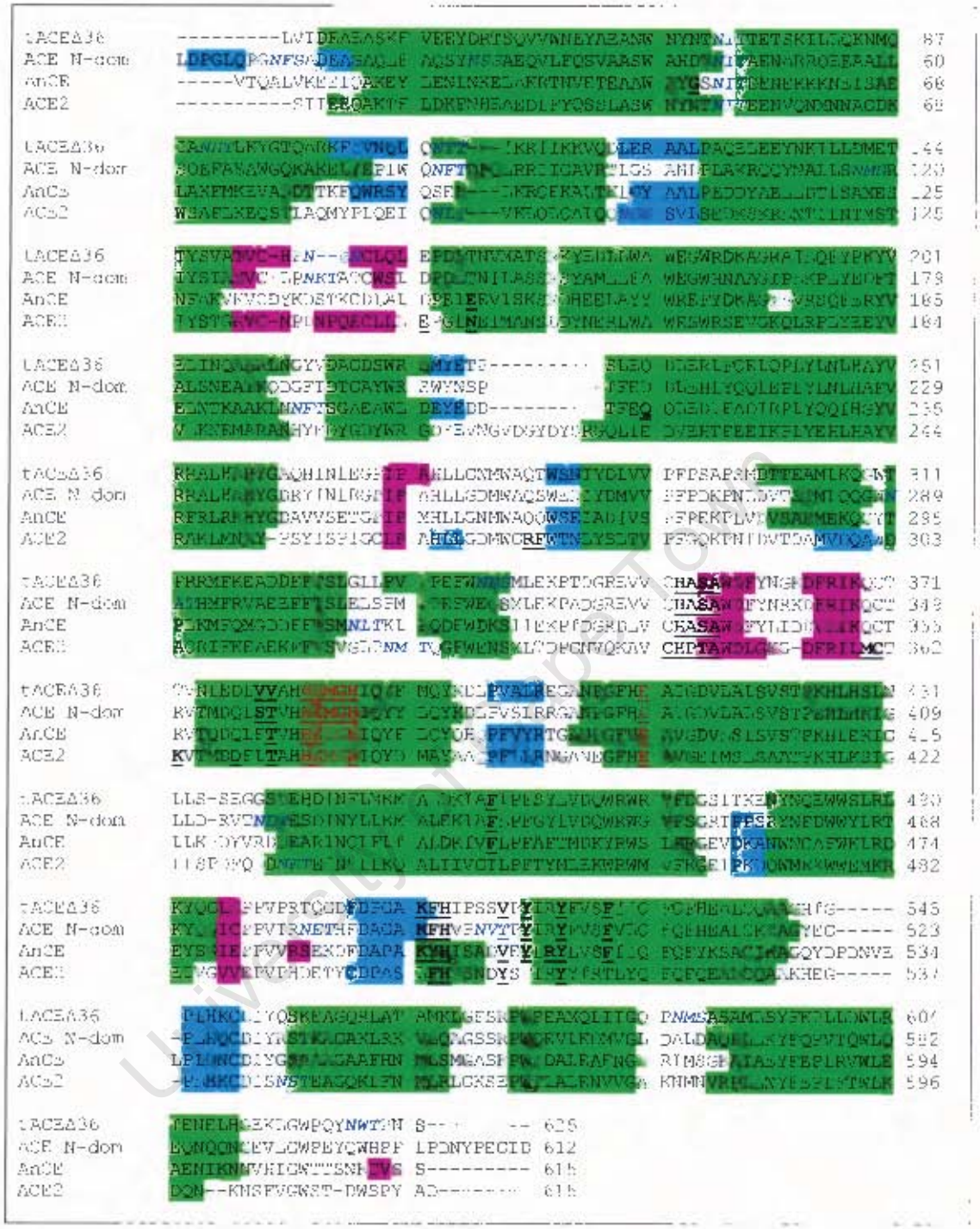

Figure 1-5. Sequence-structure alignment of human tACE, N-domain ACE, ACE2 and *Drosophila* AnCE, generated with CLUSTALW (Chenna et al., 2003). The HEXXH catalytic zinc-binding motif and zinc-coordinating glutamate are shown in red font; N-linked glycosylation sequons are in bold blue italics; residues likely to interact with ligand (distance < 5 A) are bold and underlined. Secondary structure is indicated by highlighting: α-helices in green, β-strands in purple, and 3^{10} helices in pale blue.

The zinc-binding motif, HEXXH (in tACE XX = MC) with a downstream E residue (24 residues after the second histidine) firmly places ACE with thermolysin in the gluzincin family of zinc-coordinating metalloproteases (Riordan, 2003), although it shares neither sequence nor structural similarity outside the active site with thermolysin.

The zinc ion at the active site of the native structure of tACE was found to be coordinated with the two histidines of the HEXXH zinc-binding motif, the downstream glutamate (E^{411}), and an acetate ion, which probably came from the crystallisation buffer (Natesh et al., 2003) (Fig. 1-7).

Large-scale motion between the apoenzyme and the inhibitor-bound form was not evident from the two structures, although the presence of the acetate molecule as a ligand in the native structure may have prevented such an observation. Modelling and analysis of the normal modes of tACE have revealed that there is a likely opening and closing motion about a hinge region, similar to that found in ACE2 (Towler et al., 2004; Watermeyer et al., 2006). Without this motion it is difficult to envisage how large substrates can gain access to the enclosed active site.

Lisinopril is a substituted N-carboxyalkyl dipeptide (Patchett et al., 1980) with ACE K_i values in the sub-nanomolar range (Wei et al., 1992; Jaspard et al., 1993). In the lisinopril-bound structure of tACE, the inhibitor molecule is bound in an extended conformation, with the zinc atom in this complex coordinated by oxygen of the phenyl carboxylate group, which also forms a hydrogen bond with the hydroxyl of Y^{523}. The other oxygen of this carboxylate forms a hydrogen bond with the carboxylic acid side chain of E^{384} (probably protonated as crystallisation was carried out at pH 4.7). The inhibitor residues (or analogues thereof) are named using the nomenclature first proposed by Schechter and Burger (Schechter & Berger, 1967). The phenylpropyl group (P1) is closest to the N-terminal lid helices, and makes van der Waals' contacts with hydrophobic residues. The lysyl group (P1') is parallel to the HEXXH-containing helix (α-13). The carbonyl group of the lysyl residue has clear hydrogen bonds to two histidines, H^{513} and H^{353}, while its amino nitrogen is H-bonded to the carbonyl of

A^{354} (Fig. 1-7). The lysyl side chain amine interacts with side-chain carboxylates of the S1' subsite *via* water molecules (Natesh et al , 2004). The carboxyl group of the prolyl (P2') moiety faces away from the zinc-coordination site and is H-bonded to the hydroxyl group of Y^{520} and side chain amine of K^{511} (Fig. 1-7). The prolyl group fits into the rather large hydrophobic S2' subsite surrounded by hydrophobic residue side-chains Y^{523}, F^{457} and F^{527}. Residues E^{376}, V^{379} and V^{380}, which are on the same α-13 helix as the HEXXH-motif, also occur in the vicinity of the S2' subsite occupied by the P2' prolyl.

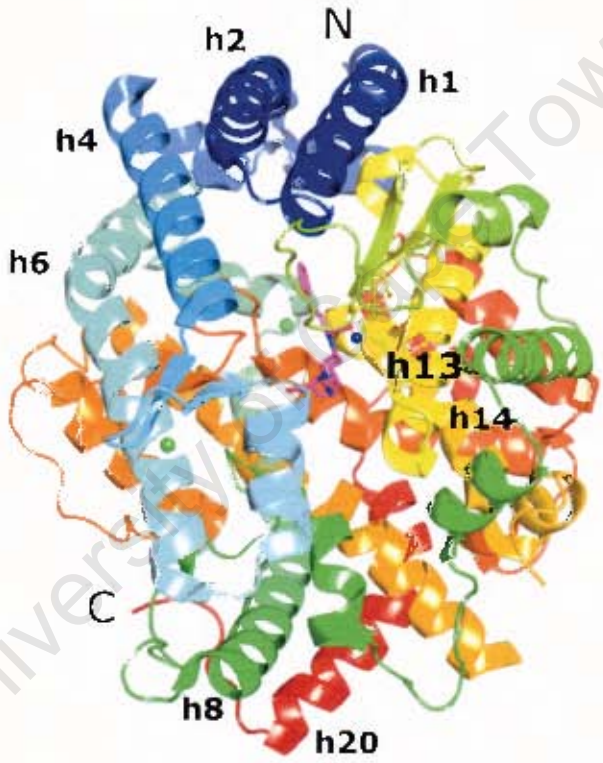

Figure 1-6. Three-dimensional structure of tACE-Δ36NJ complexed with lisinopril (purple sticks) (pdb code 1o86, (Natesh et al., 2003)). The cartoon representation is coloured in rainbow sequence (N-terminus dark blue, C-terminus in red). The catalytic zinc and bound chloride ions are represented as metallic blue and green spheres, respectively. Some of the α-helices are labelled, including the two lid helices at the top of the figure, and α-helix 13 that contains the catalytic histidines.

1.3.2.2. tACE–captopril (1uzf) & tACE-enalaprilat (1uze)

The structure of the same minimally glycosylated tACE complexed with captopril has also been determined (Natesh et al., 2004). Captopril (D-3-mercapto-2-methyl-propanoyl-L-proline) was one of the first inhibitors of angiotensin-converting enzyme to be approved clinically and commercially marketed as an antihypertensive drug (Cushman et al., 1977; Ondetti et al., 1977; Cushman & Ondetti, 1980). It is one of the smaller ACE inhibitors available, occupying only the zinc-binding site and the S1' and S2' subsites, but it binds very strongly with a K_i in the nanomolar range (Cushman & Ondetti, 1980) for both domains (Wei et al., 1992).

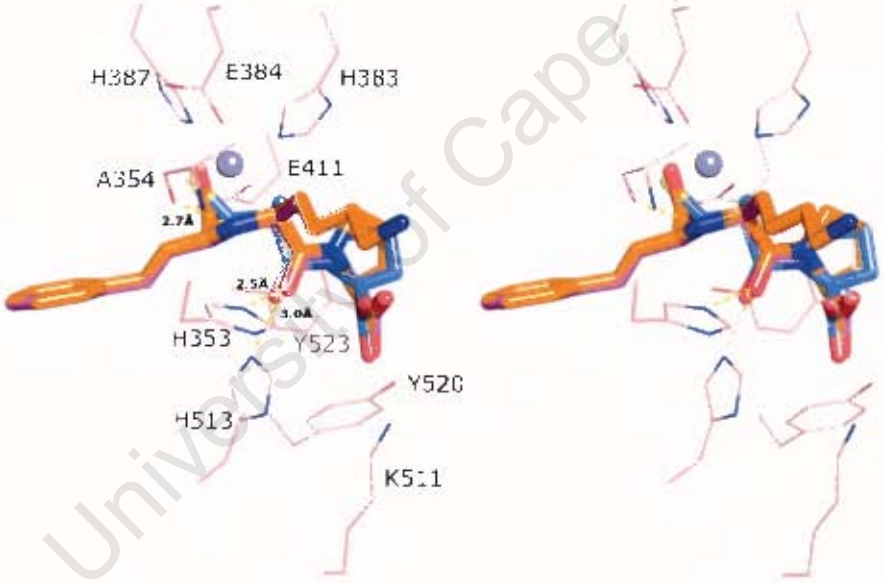

Figure 1-7. Alignment of ACE inhibitors lisinopril (orange), enalaprilat (purple) and captopril (blue) (structures from pdb files 1o86, 1uze and 1uzf, respectively). The enalaprilat is just visible as an almost-perfect superimposition on lisinopril. Active site residues and catalytic zinc (sphere) are taken from the native tACE structure (pdb code 1o8a).

The binding of the captopril molecule at the active site occurs *via* the sulphydryl and the zinc ion. Since this is not a carboxyl (as in the case of lisinopril), there is no additional coordination to Y^{523}. As with lisinopril, the carbonyl group of the P1' residue (alanine, in the case of captopril) coordinates with the histidines H^{353} and

H^{513}. The C-terminal carboxylate has much the same coordination as lisinopril. Because of its small size, the captopril molecule makes much less use of the contacts available in the S1' and S2' subsites than inhibitors such as lisinopril, and trandolaprilat.

Enalaprilat, a compound that is identical to lisinopril on the N-terminal side (*i.e.* at the P1 group), has the binding interactions that would be expected of the P1 phenylpropyl, the phenylcarboxylate and the P1' carbonyl groups. Enalaprilat is also identical to captopril on the C-terminal side (from the alanine side chain in S1'), and so the same interactions are found.

1.3.3. ACE structures – N-domain

The N-domain of ACE has been found to have different substrate and inhibitor selectivities and binding characteristics (described in the relevant sections). Experimental structures of the ACE N-domain – the native form and in complex with lisinopril – have been recently published (Corradi et al., 2006). Prior to this, a number of groups attempted to predict the N-domain structure, based on the structure of tACE (Tzakos et al., 2003; Fernandez et al., 2003) (see modelling section).

The three-dimensional structure of the N-domain to 3 Å revealed a very similar overall structure to the C-domain. Consistent with the knowledge that the N-domain is less chloride-dependent (Wei et al., 1992) only one chloride ion position was found in the structure, and this site corresponds to that of chloride II in tACE. The largest N-terminal helices form a lid structure with closely associated glycan residues, similar to that found in tACE. No conformation difference was found between the apoenzyme and the liganded form, probably for the same reason as with tACE – the presence of an acetate molecule in the native enzyme active site. The differences between the N- and C-domain active sites were found to be attributable not only to differing residues at corresponding positions (Table 1), especially in the S1' and S2' sub-sites, but also due to slight shifts in helical positions and residue side-chain orientations. For example, R^{350} of the N-domain might interfere with the lysyl group of bound lisinopril were it

orientated the same way as the corresponding T^{372} of tACE. This provides just a hint that domain selectivity may involve the interplay of several levels of related determinants, of which predicted conformational fit may be just one.

Table 1. Active site residues that differ between ACE N- and C-domains (Corradi et al., 2006).

S2	tACE/C-domain	E^{403}	F^{391}	V^{518}					
	N-domain	R^{381}	Y^{369}	T^{496}					
S1	tACE/C-domain	V^{518}	S^{516}	E^{143}					
	N-domain	T^{496}	N^{494}	S^{119}					
S1'	tACE/C-domain	E^{162}	N^{277}	S^{284}	E^{372}	N^{374}	E^{376}	D^{377}	V^{380}
	N-domain	D^{140}	D^{255}	E^{262}	R^{350}	T^{352}	D^{354}	N^{355}	T^{358}

completely deglycosylated [illegible] m453

the enzyme is relevant to its intracellular protection and stability (Williams et al., 1996).

Biochemical studies have indicated that AnCE may resemble the C-domain rather than the N-domain of ACE. For example, the AnCE hydrolysis kinetics of Ac-SDKP (a predominantly N-domain substrate) resemble those of the C-domain, and the chloride dependence with Hip-HL as substrate is like that of the C-domain (Williams et al., 1996). In addition, it appears to play a role in fertility

since knocking out the AnCE gene has a negative effect on fertility (Tatei et al., 1995).

The structure of AnCE, a homologue of ACE found in *Drosophila melanogaster*, was published soon after the tACE structure had been solved (Kim et al., 2003). The structure of AnCE is overall similar to tACE in that it is globular, hydrophobic and predominantly α-helical. AnCE shares just 42% sequence identity with tACE; however this figure exceeds 70% in the areas around the active site of the enzyme (for both tACE and the ACE N-domain) (Fig. 1-5). The catalytic residues, structure (and presumably mechanism) are conserved between the two enzymes (Williams et al., 1996; Brew, 2003; Kim et al., 2003).

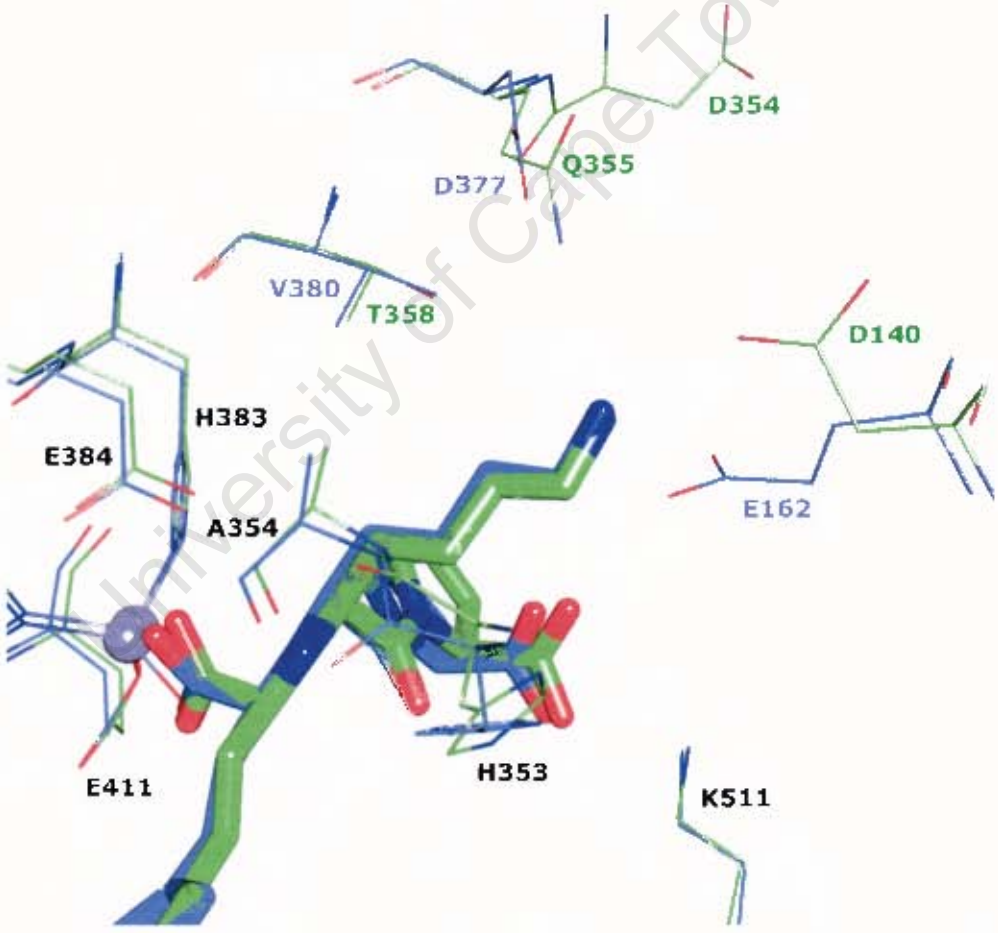

Figure 1-8. The S1' pocket of ACE. N-domain (green, pdb code 2c6n) and tACE (blue, pdb code 1o86) aligned, with residues differing between domains labelled with appropriate colour. The two aligned lisinopril molecules are shown as thick sticks.

The structure of AnCE (Kim et al., 2003) revealed a large internal channel running along the length of the entire molecule. As in tACE, the channel is composed of two chambers of unequal size, with the catalytic zinc occurring at the narrow segment between the two chambers.

The zinc ion in the native state is penta-coordinated to two water molecules, the conserved histidines H^{383} and H^{387} (tACE numbering) and the downstream glutamate E^{411} of the HEXXH...E gluzincin motif. By means of hydrogen bonding, D^{415} coordinates the zinc indirectly *via* H^{383} (Kim et al., 2003). Captopril binds AnCE with a similar nanomolar K_i to ACE. As with tACE, the sulphydryl group binds to the zinc atom, completing the distorted tetrahedral geometry with the active site histidines and glutamate. The carbonyl of the alanyl (P1') residue coordinates with two other histidines, H^{353} and H^{513}, as well as with Y^{523}. The carboxyl group of the P2' proline residue is held by hydrogen bonds and ionic interactions with Q^{281}, K^{511} and Y^{520}. All of these are conserved in both domains of sACE. It has been proposed that this "locking mechanism" restricts ACE to dipeptidase activity, except in the case of substrates that are amidated at the C-terminus (Kim et al., 2003). ACE can release the C-terminal tripeptide from such substrates, for example substance P and GnRH (Erdos & Skidgel, 1987; Ehlers & Riordan, 1989), suggesting that the peptide substrate slips in the absence of sufficient bonds to hold the carboxy group firmly in place (Kim et al., 2003).

Lisinopril binds to AnCE with a K_i of 18nM (cf. lisinopril-binding to tACE: K_i=0.2nM) (Williams et al., 1996; Kim et al., 2003). There is a similar penta-coordination found in this complex as in the enalaprilat complex, with the two oxygens of the carboxylic group coordinating zinc with the active site histidines and glutamate. The phenyl group is extended towards the N-terminal lid of the enzyme, and interestingly occurs close (3.78 Å) to an arginine residue (which was expected to be glycine, based on the enzyme sequence). This non-ideal association may partly explain the reduced lisinopril affinity of AnCE compared to tACE. The same main chain coordination occurs with lysyl in lisinopril as with alanyl in enalaprilat. The lysine side chain has water-mediated hydrogen bonds with T^{364} and D^{360}, which are V^{380} and E^{376} in tACE, and ionic interactions with

D^{360}, D^{146} and E^{150}. These correspond to E^{376}, E^{162} and T^{166} in tACE (Fig. 1-5), and are thus conservative changes.

Interestingly, though V^{380} is usually considered to play a role in the binding of the substrate via the S2' pocket, it appears that the side chain may have freedom to swing round to form part of the S1' pocket (Fig. 1-8).

1.3.4.2. ACE2 (*Homo sapiens*)

The ACE2 protein is a human homologue of ACE that has been found to play a crucial role in the regulation of heart function (Crackower et al., 2002; Danilczyk et al., 2003; Oudit et al., 2003). The ACE2 structure was determined in the absence and presence of a specific inhibitor, MLN-4760 ((*S*,*S*)-2-{1-carboxy-2-[3-(3,5-dichlorobenzyl)-3*H*-imidazol4-yl]-ethylamino}-4-methylpentanoic acid) (Towler et al., 2004). Like the tACE structure, the enzyme can be divided into two sub-domains between which runs the deep cleft in which the substrate binds. In the case of ACE2, the substrate binds at the bottom of this cleft – the cleft does not run through the entire molecule length. The two structures suggested the occurrence of a significant hinge-bending motion between the two subdomains on the binding of the inhibitor (or also, presumably, substrate).

The absence of an apparent similar hinge-bending motion between the unbound and ligand-bound tACE (Natesh et al., 2003) has been suggested to be an artifact of the experimental conditions of the crystallisation process. The native structure, determined using tACE with no substrate nor inhibitor, does not have an unoccupied active site: there appears to be an acetate molecule coordinated to the zinc, as well as an unknown molecule modelled as an N-carboxyalanine. These two molecules, bound in an orientation analogous to the inhibitor lisinopril, can be considered ligands of the native structure, and therefore preventing a true view of the unbound tACE (Towler et al., 2004).

Figure 1-9. Alignment of tACE and ACE2 showing how the S2' site is occluded by R^{273} in ACE2. The tACE active site surface is shown in white/pale grey, along with some active site residues (lines, white C atoms) and lisinopril (sticks, orange C atoms). ACE2 residues have green C atoms. The clash between R^{273} and the C-terminal carboxylate of lisinopril indicates clearly why tACE inhibitors are ineffective against ACE2.

The ACE2 and tACE structures are readily superimposable (r.m.s.d. = 1.80 Å) (Towler et al., 2004). At the active site, many residues are conserved; however, there are significant differences, some of which can be understood to contribute to the difference in function and specificity of the enzymes. For example, R^{273} in ACE2 stabilises the C-terminal carboxylate of the inhibitor MLN-4760 in the S1' position. This residue is replaced by a glutamine in tACE (Q^{281}), which also coordinates the C-terminal carboxylate of substrate or inhibitor (at S2' of the enzyme). The much greater size of the arginine residue in ACE2 (compared to glutamine in tACE) means that the potential S2' pocket in ACE2 is occluded, as shown in superimposition of tACE and ACE2 active sites (Fig. 1-9). This offers a good explanation for the carboxypeptidase activity of ACE2, as opposed to the

peptidyl dipeptidase cleavage by tACE (Crackower et al., 2002; Oudit et al., 2003). This change in the geometry of the S2' pocket also accounts for the ineffectiveness of tACE inhibitors against ACE2 (Tipnis et al., 2000; Towler et al., 2004).

1.3.5. In silico *modelling structures*

1.3.5.1. Background

Over the past three decades there have been rapid improvements in computer processing capacity and abilities to map chemical and conformational space. These have enabled the generation of reasonable models of enzymes and enzyme-inhibitor complexes based on experimentally determined structures and prior databases of chemical interactions and parameters.

The conformations of inhibitors at the active site of ACE were predicted nearly two decades ago using available data from the structures of several known active inhibitors (Mayer et al., 1987). Recently, it was shown that the active site model prediction was indeed highly accurate, when compared to the published ACE-inhibitor complex structures (pdb codes 1o86, 1uze, 1uzf – ACE-lisinopril, -enalaprilat and -captopril, respectively). It was suggested to be the earliest example of such validation, and exemplified in support of the methodology of active site mapping using known active analogues/inhibitors. Active site mapping is a most useful approach in the absence of three-dimensional structural information about a protein target. If a set of inhibitors of sufficient chemical diversity has been characterised, then important geometric parameters of the active site can be accurately estimated. This is based on the assumption of the narrow geometric constraints present at active sites, enabling substrates to be held in particular conformation for catalysis (Kuster & Marshall, 2005).

The development of numerous software applications specific to biological macromolecules has resulted in the rapid growth and progress of the field of molecular modelling. CLUSTALW is an example of a program that allows

alignment of protein domains with high homology (Chenna et al., 2003) (Fig. 1-5). Software applications such as MODELER (Sali & Blundell, 1993) or CHARMM (Brooks et al., 1983), can be used to construct models of the sample protein based on its sequence and determined similarity to a template. In the case of docking of small molecules – typically inhibitors – there are many software suites, such as AutoDock (Goodsell et al., 1996) and ZDOCK (Chen et al., 2003), that facilitate (amongst other things) the creation, and docking of molecules into macromolecules, and subsequent refinement of the interaction between them.

1.3.5.2. ACE-inhibitor docking and modelling

Various docking software suites have been employed to support or rationalise experimentally determined inhibition data, or to motivate for the modification of well-established inhibitors in order to promote domain selectivity. In this quest the Accelrys package INSIGHT II (Accelrys, San Diego CA, USA) has been used successfully in our laboratory in modelling the conformations of various inhibitors bound to the active sites of ACE (Nchinda et al., 2006a, 2006b). Other groups have used CHARMM (Brooks et al., 1983) to surmise about the interactions of the C-domain selective RXPA380 with ACE (Georgiadis et al., 2004) and MODELER (Sali & Blundell, 1993; Marti-Renom et al., 2000) to achieve results that have provided molecular insights into the determinants of selectivity in the binding of a range of current and potential clinical inhibitors of ACE (Tzakos & Gerothanassis, 2005).

1.3.5.3. ACE N-domain docking and modelling

The model of ACE N-domain bound to lisinopril indicated a similar binding structure for the two ACE domains (Fernandez et al., 2003). The zinc ion is penta-coordinated to the conserved active-site histidines and glutamate, as well as the carboxylate oxygens of the inhibitor or substrate. The glutamate residue occurring in the active site HEXXH motif (E^{362}, standard N-domain numbering

according to Corradi et al. (2006)) plays a role in coordinating the catalytically important water molecule (water385), as well as the lisinopril carboxylate.

As in the C-domain crystal structures, the P1 phenyl group interacts via aromatic stacking with the side chain of F^{490} (corresponding to F^{512} in tACE). The lysyl main chain amine binds the carbonyl of an alanine residue; the prolyl side chain fits easily in the large hydrophobic S2' pocket, while its carboxylate is coordinated to K^{489} (K^{511}) and Y^{498} (Y^{520}). The major differences occur in the binding of the lysyl side chain, where the D^{377} and E^{162} of tACE are replaced by Q^{355}, D^{354} and D^{140} (Fig. 1-8). The distance between lysyl and side chains is greater, so these interactions are likely water-mediated (Fernandez et al., 2003).

From their structure, Tzakos et al. (2003) also speculated that a series of significant residue changes in the S1 and particularly S1' pockets may contribute significantly to the substrate and inhibitor specificities. In addition they found a more positively charged binding groove for N-domain, based on surface potential calculations.

1.3.5.4. C-domain ACE-inhibitor models

Although the crystallisation and structure determination of ACE complexed with three inhibitors has been demonstrated, it has so far proved to be a difficult procedure to reproduce. It must also be noted that at least 17 ACE inhibitors have been approved for clinical use (Zaman et al., 2002). Therefore details of the mode of binding have only been elucidated for a small fraction of commercially available inhibitors. It is expected that such detailed information would be particularly useful in the modification of current inhibitors in the quest to obtain domain-selective inhibitors – it would allow the delineation of the factors to be exploited in order to attain domain selectivity. Understanding these factors can guide the design of second-generation domain-selective inhibitors.

With this in mind, Tzakos and Gerothanassis (2005) have determined the binding modes of a number of ACE inhibitors in complex with both the C-domain and the

N-domain (generated using MODELER). The results for the calculated complex of C-domain ACE and lisinopril agreed well with the experimentally determined structure, giving credence to the results for the other docked structures.

1.4. Rationale of the Study

1.4.1. Domain-selective inhibition

Most commercially available inhibitors were designed before the discovery of the two domains, and have turned out to be efficient at inhibiting both domains to roughly similar extents.

Since the discovery of the two domains of ACE, studies that have strongly suggested that C-domain inhibition is both necessary and sufficient to produce an anti-hypertensive effect have encouraged investigations into the development of C-domain selective inhibitors. For example, Bernstein and others have shown in mice that the N-domain alone cannot restore low blood pressure to normal levels (Esther et al., 1997), while the administration of an N-domain specific inhibitor, RXP407, had little effect on angiotensin hydrolysis by sACE (Dive et al., 1999; Junot et al., 2001). Furthermore, C-domain-selective inhibition will allow BK degradation by N-domain, preventing BK accumulation seen in angioedema. Finally, because BK potentiation *via* B2 receptor resensitisation is highest when both domains are inhibited, an inhibitor targeting the C-domain may have a lower proclivity for excessive BK stimulation (Acharya et al., 2003).

1.4.2. Structural determinants of selectivity

The lysyl side chain of lisinopril makes contact with acidic residues in the S1' pocket. The S1' pocket does not appear to be of major importance for domain selectivity, for the following reasons. Lisinopril is roughly equally effective against both domains. In addition, the S1' residues are moderately conserved between C- and N-domains: $D^{377}Q$ and $E^{162}D$. Inhibitors such as RXPA380 have been

developed with special consideration given to S2' pocket-based (C-domain) selectivity (Acharya et al., 2003; Georgiadis et al., 2004). Trandolaprilat, whose design (before the discovery of the two-domain nature of ACE) was based on enalaprilat, also has a bulky aromatic group (indole ring) at its P2' position, and this inhibitor was also found to be moderately C-domain selective (Wei et al., 1992).

The inhibitor RXP407 demonstrated a 1000-fold selectivity for the N-domain, while RXPA380 has shown a 3300-fold selectivity for the C-domain (Dive et al., 1999; Junot et al., 2001; Georgiadis et al., 2003; Georgiadis et al., 2004).

The remarkable selectivity of RXPA380 seems to have its basis in the interactions with the enzyme that occur in the P2' position, occupied by a tryptophan residue (Fig. 1-10). Mere replacement of the tryptophan side chain with a methyl group or pseudo-arginine (to form the analogue Compounds 8 and 11, respectively) reduced selectivity in both cases from 3300-fold to 22-fold, fully two orders of magnitude. The analogue Compound 9, with methyl groups at both P1' and P2', despite showing high affinity for ACE, exhibits no selectivity whatsoever. Furthermore, the carboxybenzyl moiety that occupies the S2 pocket of the enzyme appears important for binding, but does not seem to play a direct role in the selectivity of the inhibitor, as modifications of inhibitor structure at the P1' and P2' positions appear sufficient to eliminate or enhance C-domain selectivity (Georgiadis et al., 2004).

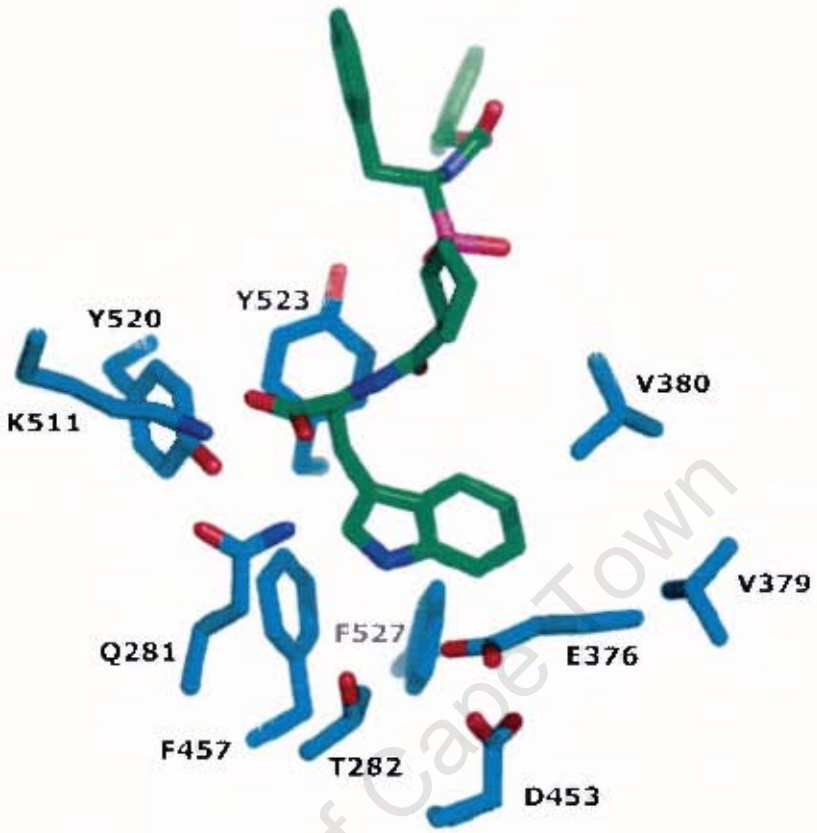

Figure 1-10. Prediction of S2' pocket configuration by Georgiadis *et al.* Of the 12 residues predicted to be within 5 A of RXPA380 tryptophan side chain, D^{415} and F^{466} are not shown. K^{511} is shown for clarity(Georgiadis et al., 2004).

Modelling of RXPA380 docked into the active site of tACE-lisinopril structure (replacing lisinopril) has suggested that the interactions of the tryptophan at P2' are specifically critical to selectivity. The lysine residue at P1' in lisinopril of the tACE-lisinopril structure (1o8a) has been found to have unusual phi and psi angles that are in fact typical for a proline residue. This observation is supported by the ease with which the pseudo-proline at P1' in RXPA380 is modelled – the two residues correspond closely. The interactions of the pseudo-proline are with A^{354} and H^{353}, which come from a highly conserved region of ACE, and therefore it appears that these interactions cannot explain domain selectivity.

On the other hand, of twelve residues defined by Georgiadis et al (2004) as comprising the S2' subsite, five differ between N-domain and tACE [C-domain]

The major differences are the replacements of hydrophobic valines V^{379} and V^{380} by serine and threonine, respectively, and the conversion of acidic residues – $E^{376}D$ and $D^{453}E$. These changes may sterically interrupt the possible H-bond interaction between the nitrogen of the indole ring of the P2' tryptophan and the D^{453} carboxylate in tACE.

1.4.3. Project Aims

Although these findings provide some explanations, further structural data are required in order to gain definitive insights into the interactions mediating such selectivity, and these data may even point to mechanisms associated with the selectivity. There are at least two currently tractable ways to achieve these insights: co-crystallisation of RXPA380 with tACE or the C-domain of ACE, or structural determination of a tACE [C-domain] mutant containing N-domain residues in the key positions, preferably co-crystallised with lisinopril or RXPA380. We have adopted the former approach, and expect this to shed light on the factors determining selectivity in the C-domain.

Therefore the aims of this project are:

1. Determination of the conditions that are conducive to the production of diffraction-quality and -size crystals of minimally glycosylated tACE-inhibitor complexes;
2. Co-crystallisation of tACE with the C-domain-selective inhibitor RXPA380, X-ray diffraction data collection, and solution and refinement of the structure of tACE complexed with RXPA380;
3. Modelling *in silico* of the tACE–RXPA380 interaction for comparison of the modelled interactions with those in the crystal structure.

2. MATERIALS AND METHODS

2.1. Protein expression

Testis ACE (tACE) mutants with reduced glycosylation were previously produced by site-directed mutagenesis and stably transfected into Chinese Hamster Ovary (CHO) cells (Gordon et al., 2003). The mutants used in this work were the tACE-g13 and tACE-g3 mutants, which have only two (1st and 3rd) and one (3rd) glycosylation sequons intact, respectively. CHO cells were cultured in medium composed of equal amounts of Dulbecco's Modified Eagle Medium (DMEM) and Ham's F12 (Highveld Biological, Lyndhurst, RSA), 2% foetal calf serum (Gibco BRL, Life Technologies, UK), and 0.02M HEPES as described previously (Ehlers et al., 1991a). The medium was harvested at ~3 day intervals for 14-16 days after the first induction with $ZnCl_2$. After the first two passages with 2% FCS medium some of the T150 flasks were exposed to 2% FCS medium containing the α-glucosidase I inhibitor *N*-butyldeoxynojirimycin (NBDNJ). The bulk of the medium was stored at -20°C, with 1 mL aliquots removed in order to carry out ACE activity assays.

2.2. Purification by affinity chromatography

Medium containing tACE-g13 mutant protein was passed over a lisinopril-Sepharose affinity column at a rate of 1.1 mL/min using a Gilson Minipuls2 pump (Villiers-le-Bel, France). The entire flow-through was retained and assayed for ACE activity. The column was washed overnight with wash buffer (20 mM Hepes, pH 7.5 containing 0.3 M NaCl) and eluted with 50 mM sodium borate (pH 9.5). An in-line spectrometer (D-Star Instruments, VA, USA) measured absorbance of the eluted fractions at a wavelength of 280 nm.

2.3. Enzyme activity assays

The eluted fractions were pooled and dialysed against 5 mM HEPES pH 7.5 containing protease inhibitor (0.1 mM PMSF, Roche Diag. GmBH, Germany) for 24-36 hours.

The enzyme activity of the dialysate was measured using hippuryl-histidyl leucine (HHL) as substrate (Friedland & Silverstein, 1976). Briefly, dialysate aliquots were incubated at 37°C for 15 minutes with the substrate HHL. The reaction was stopped by placing the tubes on ice and adding 750 µL of 0.28 M NaOH. 50 µL of 8 mM *o*-phthaldialdehyde was added, and the sample was left for 10 min to allow formation of the fluorescent adduct from the reaction between the *o*-phthaldialdehyde and the primary amine of the histidyl moiety of HL that results from ACE activity.

The dialysate (or aliquot of each fraction, or of harvested medium) was diluted appropriately so that the fluorescence reading would fall within the acceptable detection range. In the case of the medium activity assays, five- or ten-fold dilutions were carried out in order to minimise the effect of quenching of the fluorescence signal due to the presence of many other proteins and other organic material in the harvested medium samples.

2.4. Protein concentration

A 4mL volume ultracentrifuge tube (Millipore, MA, USA) was washed with 5mM HEPES. The dialysate was placed into the tube over the filter, and centrifuged at 4500 × *g* until the desired concentration was reached. The protein content was determined using a standard Bradford assay (BioRad Laboratories GmbH, Germany). The concentrated ACE was stored at 4°C. To check the purity of the concentrated enzyme, between 3 µg and 20 µg of the sample was electrophoresed on 10% SDS-PAGE.

2.5. Crystallisation

2.5.1. General crystallisation conditions

Crystallisation (or reservoir) buffer was prepared as done previously (Gordon et al., 2003; Watermeyer et al., 2006). The buffer solution consisted of 15% polyethylene glycol (PEG) 4000 (Fluka Chemie GmbH, Switzerland), 50 mM

hydrated sodium acetate (Merck, Darmstadt, Germany), and 10 µM hydrated zinc sulphate. The pH of the buffer was adjusted to between 4.4 and 5.0 with HCl and NaOH using a Beckman pH machine (Beckman, Irvine CA, USA). The buffer was filter-sterilised (0.22 µm filter) and stored at 4°C.

Typically, drops of volume 4 µL were placed onto each cover slip (2 µL protein or (protein + inhibitor) mixed into 2 µL reservoir buffer) and inverted over a 1 mL reservoir buffer volume (the hanging drop method). This was optionally overlaid with 0.5 mL of a 1:1 mixture of silicon:paraffin oils (Hampton Research, Aliso Viejo CA, USA).

Crystallisation trials were set up at an ambient temperature of 18-21°C in an attempt to minimise condensation on the cover slips. Plates were placed in a low-temperature incubator (United Scientific, Cape Town, RSA) at 16°C, atop three layers of packing foam (~4 cm total thickness) in order to minimise interference with crystal formation by vibrations of the incubator.

2.5.2. Initial tACE-g13–RXPA380 co-crystallisation conditions

The range of inhibitor concentrations used initially was such that a final (in-drop) concentration of between 3 nM and 1 µM was used in the crystallisation trials. The final in-drop protein concentration was either ~0.75 mg/mL or ~1.65 mg/mL, which correspond to approximately 10.5 µM and 23 µM, respectively.

2.5.3. Final tACE-g13–RXPA380 co-crystallisation conditions

Crystals of native tACE-g13 (the original in-drop concentration was 1.65 mg/mL) were dissolved by transferring the cover slip to a well containing only distilled water. After 24 hours, 1 µL of 0.46 mM RXPA380 was added to the 4 µL, drop. This resulted in an effective concentration of ~0.1 mM of the

inhibitor. The cover slip was then re-transferred to the well containing the appropriate reservoir buffer, as before.

2.6. Data collection and processing

Crystals were visually inspected for quality, and their dimensions were measured using an in-lens graticule on a stereomicroscope (Leica Microsystems, Wetzlar, Germany). Images were acquired on a Leica Z16 APO (KLI500 LCD) stereomicroscope connected to a computer, using the IM500 program (Leica Microsystems, Wetzlar, Germany).

2.6.1. In-house data collection and processing

Preliminary diffraction data from the best crystal produced using the initial co-crystallisation conditions were collected on the in-house X-ray diffraction machine at the University of Western Cape, South Africa. The X-ray diffraction machine consists of a Rigaku RUH3R copper rotating-anode X-ray source operated at 40 kV, 22 mA; a Rigaku R-axis IV+ image plate camera (Rigaku MSC, Tokyo, Japan); an X-stream 2000 low-temperature system (Rigaku MSC, Houston TX, USA); and an AXCO PX50 glass capillary optic with a 0.1 mm focus (Australian X-Ray Capillary Optics, Parkville VIC, Australia).

Images were collected between 0° and 180°, with an oscillation angle of 0.5° per frame, to make a total of 360 data frames. The exposure time for each frame was 600 s. The detector-to-crystal distance was set at 100 mm, and later refined to 102 mm.

The image frames collected were indexed and integrated with Denzo and scaled and merged with SCALEPACK (Otwinowski & Minor, 1997). Molecular replacement using EPMR v2.5 (Kissinger et al., 1999) and the structure of native tACE-g13 (Watermeyer et al., 2006) as starting model was carried out

to obtain an initial model with phases. Data in the resolution range 15 – 4 Å were used in the evolutionary search procedure.

Model refinement was carried out using input scripts (modified as required) of the Crystallography and NMR System (CNS) v1.1 (Brunger et al., 1998).

2.6.2. Synchrotron data collection and processing

Testis ACE-g13–RXPA380 co-crystals, produced using the final co-crystallisation conditions, were transported in trays to the European Synchrotron Radiation Facility (ESRF) at Grenoble, France. The crystals were observed again under a microscope to ensure that there had been no loss or damage in transit. The selected crystal was picked and soaked briefly in a mixture containing 80% reservoir buffer and 20% glycerol, acting as cryoprotectant. Each crystal was then placed in a special labelled vial containing liquid nitrogen. Ten of these vials were slotted into a cartridge (or "puck") for storing the crystals within the microdiffractometer.

Diffraction data were collected on the BM14-UK beamline at ESRF, using radiation of wavelength of 1.033 Å with maximum intensity of ~7.5 × 10^{11} photons. The beam had a focal area of 0.25 mm^2. Diffraction images were recorded on the MARMOSAIC225 charge-coupled detector, and had an area of 225 mm × 225 mm. Images were collected between 0° and 144° with an oscillation angle of 1.0° per frame, to make a total of 144 data frames. The exposure time for each frame was 40 s. The detector distance was set at 193.8 mm.

The image frames collected were indexed, integrated, scaled and merged with HKL2000 (Otwinowski & Minor, 1997). Molecular replacement using EPMR v2.5 (Kissinger et al., 1999) was carried out to obtain an initial model with phases. The structure of native tACE-g13 (Watermeyer et al., 2006) was used as a starting model. Data in the resolution range 15 – 4 Å were used in the evolutionary search procedure.

2.7. Structure refinement

Model refinement was carried out using input scripts (modified as required) of CNS v1.1 (Brunger et al., 1998). An initial *B*-factor correction was employed in each refinement round, with a low-resolution limit of 6.0 Å. A general bulk solvent correction was also automatically determined and used. Coordinate minimisation was carried out using a maximum likelihood target with structure factor amplitudes. A relative weighting for the X-ray term was automatically determined and applied. An automatic weighting term was also applied during *B*-factor minimisation.

Difference $F_{obs} - F_{calc}$ and $2F_{obs} - F_{calc}$ maps were calculated using coefficients calculated from sigmaa weighting. A test set of 776 reflections (3.7% of the total) was excluded from all refinements, and was used to calculate the R_{free} statistic. Inspection of maps and models and model building was all carried out in *O* (v10.0) (Jones et al., 1990).

After the first round of refinement, the program Mapman (Kleywegt & Jones, 1996) was used to locate the zinc and chloride ion peaks. These locations were confirmed by inspection in *O*. Group *B*-factors were refined (with each residue treated as two parts, main chain and side chain). Water molecules were added gradually to the model with Mapman and generally searching for peaks above 4σ in the $F_{obs} - F_{calc}$ map. These were confirmed or added to using the CNS script water_pick.inp, and checked in *O*, by ensuring that reasonable hydrogen bond donors and acceptors were available to the putative waters. In later rounds of refinement some peaks above 3σ and 2.5σ were also used.

In order to obtain coordinates for the glycan residues, a C_α-alignment of the model to a complete native tACE-g13 structure was made. Glycan residues at N^{72} (g1, one glycan) and N^{109} (g3, up to five glycans) were then adjusted to fit the observable difference density. Later on in refinement, the glycan at N^{72} and one of the outermost glycan residues at N^{109} (a mannose) were removed

because of unclear density and very high *B*-factors suggesting only partial occupancy or a high degree of flexibility.

The inhibitor RXPA380 (Georgiadis et al., 2004) was built from the available chemical structure and stereochemical details using the ProDRG server (Schuttelkopf & van Aalten, 2004). The server also generated the molecule's topology and parameter files for use in CNS, and minimised the structure for the first manual "docking" into the active site. The minimised structure was then manually placed into the active site using tools in *O*. Permitted torsion angles of the molecule were adjusted in order to fit the electron density as seen in the difference map.

In subsequent model building the cis- and trans- conformations of the peptide bonds were checked, although the peptide torsion angles were not altered. The inhibitor was fitted until no positive peaks above 1.8σ in the $F_{obs} - F_{calc}$ map remained, and no significant negative density peaks (indicating atoms in the model not accounted for by the density map) were discernible.

The cycles of refinement were concluded when they resulted in no further substantial improvements in the map phasing and no further decrease in both the R_{free} and R_{cryst}.

2.8. Structure validation and analysis

The MolProbity server was used to switch asparagine, glutamine and histidine side chains by 180° where the analysis of nearby contacts and hydrogen bonding network supported such a switch (Davis et al., 2004). Ramachandran, rotamer and C_β plots were also generated and checked. PROCHECK was used to generate Ramachandran plots and other stereochemical plots that give indication of the quality of the model (Laskowski et al., 1993).

Alignments of the ACE-RXPA380 model with previously determined structures were carried out using PyMOL (DeLano, 2002).

The CASTp server was used to calculate the volume of the active site cavity in tACE-g13–RXPA380 with a probe size of 2.5 Å (Binkowski et al., 2003). This was compared with the N-domain structure.

2.9. Modelling: Docking and molecular dynamics of RXPA380 in active site of tACE

Files of the testis ACE complexed with lisinopril (1o86.pdb) and of the N-domain complexed with lisinopril (2c6n.pdb) were used as the starting points. These were accessed and processed on a Silicon Graphics (SG) Octane workstation (Silicon Graphics, Mountain View, CA, USA) using INSIGHT II version 2000 (Accelrys, San Diego, CA, USA).

Files were prepared for cycles of energy minimisation and dynamics by appropriate adjustment using the Builder module of INSIGHT II. Atom hybridisation and potential values were set appropriately. The consistent valence force field (CVFF, filename cvff.frc) was applied. Because INSIGHT II is not set up to recognise and incorporate the Zn^{2+} in its calculations, an appropriate substitute ion was chosen – Mg^{2+}. In order to fix its position, the active site cation was bonded to the coordinating histidines, H^{383} and H^{387}.

The phosphinate inhibitor RXPA380 (Dive et al., 1999; Dive et al., 2004) was built into the active site with lisinopril as the starting template and using the INSIGHT II Builder module. Measure functions in the Viewer module were used to identify probable steric clashes between new inhibitor structures and the protein. The inhibitor moieties were then manually adjusted so as to be in as sterically favorable orientations as possible.

The inhibitor and metalloprotease were combined into a single assembly for the molecular modelling steps. The Discover_3 module was used for all energy minimisation and molecular dynamics steps. The protocol used was the following:

- 2000 steps of Polak-Ribiere conjugate gradient minimisation
- 2000 cycles of molecular dynamics using Velocity-Verlet integration method (time-step = 1 fs)
- Compilation of a history of the configurations at an interval of 10 cycles, i.e. 200 frames
- Determination of average conformation from history trajectory;
- 3000 steps of Polak-Ribiere conjugate gradient minimisation applied to this average conformation.

All experiments were carried out at constant volume (NVT), at a constant temperature of 300 K, with a dielectric constant of 1, and *in vacuo*. Water molecules were also excluded. The non-bonded cut-off for molecular dynamics was 9.5 Å (Nchinda et al., 2006a, 2006b).

The output conformation was written out to a pdb file for further analysis. Ramachandran plots were drawn using MolProbity (Davis et al., 2004) and PROCHECK (Laskowski et al., 1993). To aid with evaluation, these were compared to corresponding analyses of tACE–lisinopril (pdb code 1o86) and ACE N-domain–lisinopril (2c6n) (for C- and N-domains, respectively). An all-molecule $C_\alpha$alignment to the ACE C-domain (1o86) was then carried out and a r.m.s.d. value was calculated. An active-site alignment, using the 20 active site residues within 5 Å of lisinopril in the PDB structure, was also carried out in order to provide a comparable illustration of the inhibitors bound in the active site. All alignments and molecular figures were generated using PyMOL (DeLano, 2002).

The key residues surrounding the inhibitor side chain groups at each subsite were consequently determined.

3. RESULTS AND DISCUSSION

3.1. Protein expression & purification

Medium harvested from tACE-g13 and tACE-g3 CHO cells was assayed using HHL as substrate. The specific activity of the medium was 142 mU/mL (total volume = 340 mL) and 89 mU/mL (total volume = 450 mL) for tACE-g13 and tACE-g3, respectively (1 mU defined as 1 nmol HL produced per minute).

tACE-g13 and tACE-g3 were purified from culture medium using a lisinopril-Sepharose column. The pre-column and post-column aliquots were assayed in order to determine ACE yields. For both tACE-g3 and tACE-g13 the yields were over 50%, indicating recovery of sufficient tACE to proceed with crystallisation experiments.

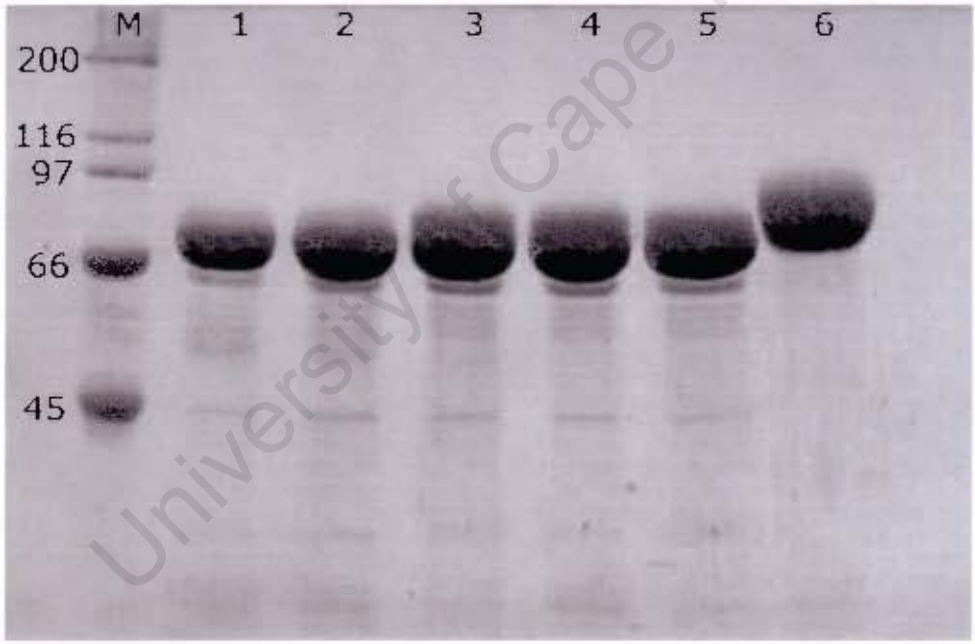

Figure 3-1. 10% SDS-PAGE showing effect of removal of glycosylation sites from tACE. Between 10 and 20 µg of protein was loaded per lane. Marker lane (M) molecular weights are in kDa. Lanes 1-2: 10 µg and 15 µg tACE-g3, respectively. Lanes 3-5: 20 µg per lane of different preparations of tACE-g13. Lane 6: 20 µg fully glycosylated tACE. The faint bands below the major bands collectively comprised less than 5% of the protein loaded per lane.

The protein concentrations of the post-column fractions after dialysis were 0.158 mg/ml (total of 1.42 mg) and 0.191 mg/ml (total of 1.20 mg) for tACE-g13 and tACE-g3, respectively. SDS-PAGE showed the dominant tACE-g13

protein had a molecular weight of 72 kDa (Fig. 3-1, lanes 3-5) which was slightly lower than the fully gycosylated tACE (Fig. 3-1, lane 6). The tACE-g3 protein bands (Fig. 3-1, lanes 1 & 2) also ran lower than the fully glycosylated tACE band, indicating similarly reduced glycosylation as expected. Minor proteins comprised ≤5% of the total protein. The tACE protein recovered in dialysate after purification gave a final yield of 4.2 mg/L and 2.7 mg/L for tACE-g13 and tACE-g3, respectively.

3.2. Crystallisation

Initial parameters for crystallisation conditions were obtained from previous work successfully carried out on tACE-g13 (Gordon et al., 2003; Watermeyer et al., 2006).

3.2.1. Crystallisation of tACE-g3

Aliquots of tACE-g3 were concentrated to 2.0 mg/mL and 4.2 mg/mL, as determined by Bradford assays. The final concentration of tACE-g3 in the drop was 2.1 mg/mL. Clusters of needles, or alternatively, microcrystal showers were obtained (Fig. 3-2). Seeding was found to be a promising approach for increasing the size of tACE-g3 crystals; however, these experiments failed to yield diffraction quality crystals.

3.2.2. Initial co-crystallisation of tACE-g13–RXPA380 complex

Aliquots of tACE-g13 were concentrated to various extents, from 0.5 mg/mL to 6.6 mg/mL, as determined by Bradford assays. Production of native tACE-g13 diffraction-size crystals was achieved with final (i.e., in-drop) protein concentrations ranging from ~0.25 mg/mL to 3.3 mg/mL. Crystals appeared gradually between 2 and 7 days after screens were set up. A fine precipitate was consistently observed to form before any crystals and remained after crystallisation had occurred.

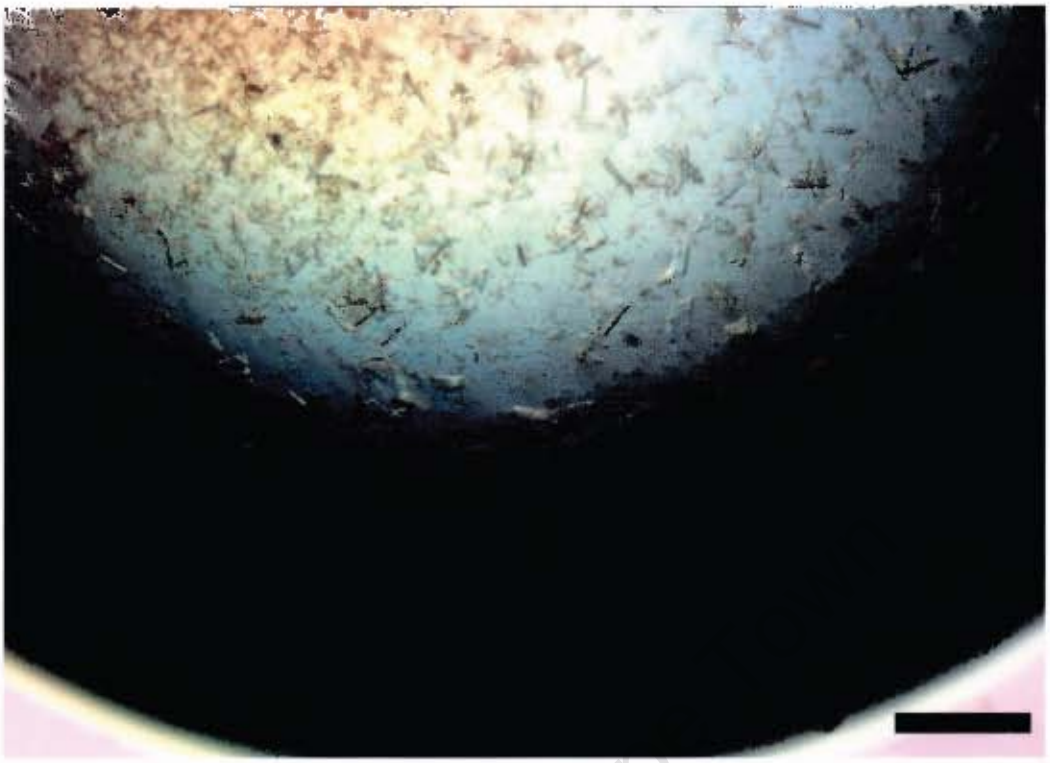

Figure 3-2. Microcrystals of tACE-g3 (1.4mg/mL) together with a considerable amount of precipitate. Scale bar indicates 0.2 mm.

A 1.6 mg/mL final concentration of protein (23 μM) was used for the enzyme-inhibitor co-crystallisation screens. Inhibitor concentrations varied from 3 nM (the K_i value for RXPA380) to 1 μM (a 333-fold excess of the inhibitor). The largest crystals were typically about 0.35 mm × 0.04 mm in the visible dimensions.

3.2.3. Final co-crystallisation of tACE-g13–RXPA380 complex

The concentration of the inhibitor in the co-incubation was increased. There is precedent for this approach – the co-crystals of tACEΔ36NJ with lisinopril (~180 μM) and with enalaprilat (10 mM) and captopril (10 mM) used for structural determination all had excesses of inhibitor at least five orders of magnitude higher than their inhibition constants (Natesh et al., 2003; Natesh et al., 2004).

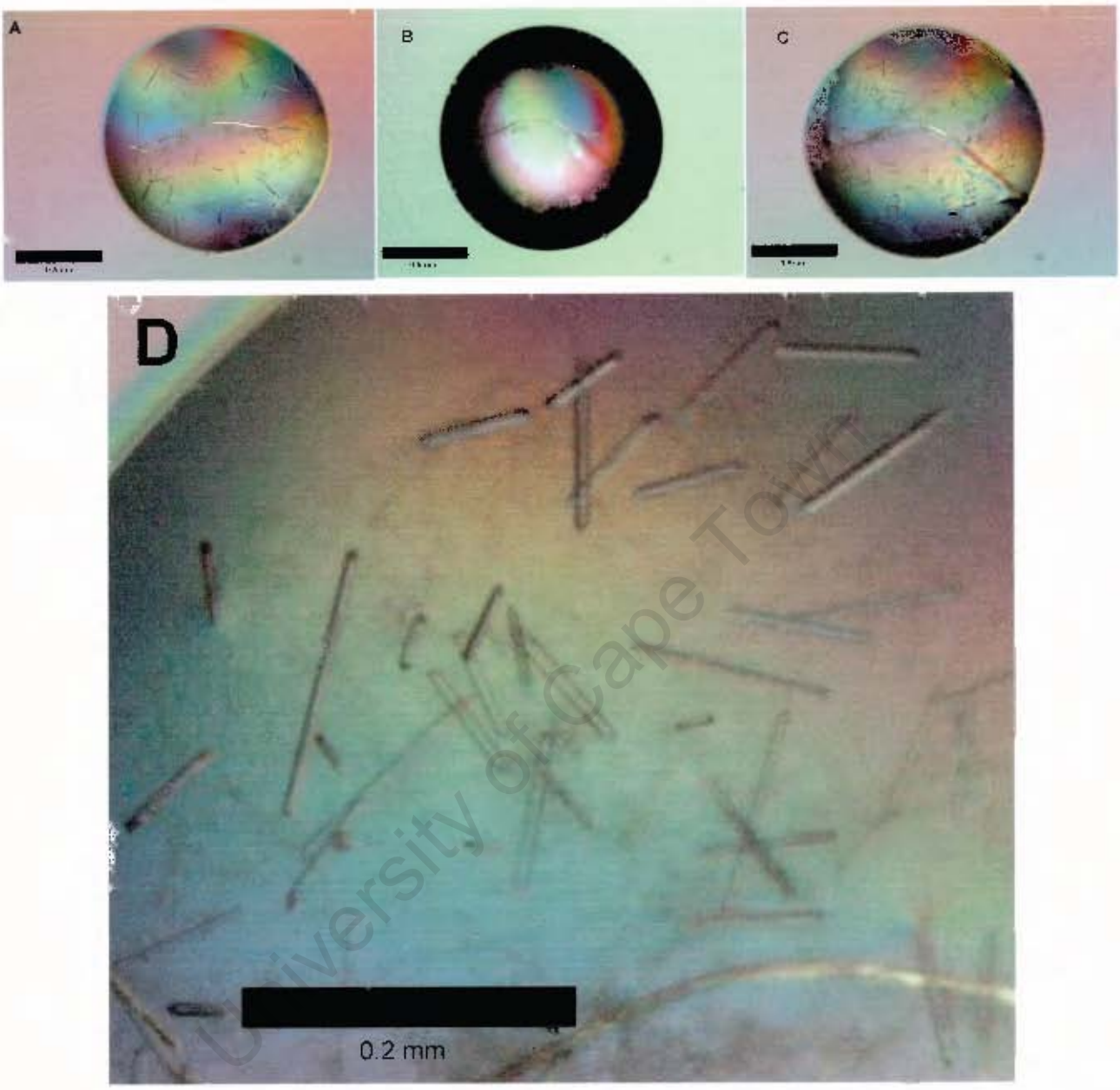

Figure 3-3. Re-crystallisation of tACE-g13 crystals in presence of RXPA380. A. tACE-g13 native crystals. B. The crystals had dissolved 48 hours after replacing reservoir buffer with water. C. Within four days of the addition of 460µM RXPA380 and replacement of water with the regular reservoir buffer (15% PEG4000, 50mM Na-acetate, 10µM Zn-sulphate), crystals had re-formed. D. Magnification of quadrant of crystallisation drop (from C). Substantial precipitate is easily observed along with well-formed needle-shaped crystals. (Bottom right is a fibre, probably from clothing)

The concentration of RXPA380 used in the enzyme-inhibitor incubation was therefore increased to give a final in-drop concentration of 92 μM, which is a ~30700-fold excess relative to the K_i value, and an inhibitor–enzyme molar ratio of 4:1. This was achieved by dissolution and re-crystallisation of native protein crystals in the presence of 0.46 mM RXPA380. This approach was used, rather than using fresh protein sample, as this protein was clearly amenable to crystallisation. Soaking was not used as it is thought that substrate/inhibitor access occurs *via* a conformational change (by hinge movement) that is both masked and prevented by crystallisation, so that inhibitor may not have access to the active site after crystallisation (Towler et al., 2004; Watermeyer et al., 2006). The crystals produced were noticeably smaller than the original crystals, with dimensions of approximately 0.2 mm × 0.02 mm for the largest crystals (Fig. 3-3).

3.3. Data collection and processing

3.3.1. In-house data collection and processing

In total 424220 diffraction spots were recorded, and these data were indexed, integrated, scaled and merged with Denzo and SCALEPACK programs (Otwinowski & Minor, 1997) to yield 104529 reflections to 2.8 Å. 17739 unique reflections were obtained, with R_{symm} = 26.1%, I/σ = 3.4, mosaicity = 0.68.

The structure was solved using molecular replacement with EPMR v2.5 (Kissinger et al., 1999), with a correlation coefficient of 0.713 and R-value of 0.575. A view of the initial Fourier difference $F_{obs} - F_{calc}$ map gave no discernible evidence for the presence of the inhibitor bound to the tACE active site. Therefore structure refinement was discontinued for these data.

3.3.2. *Synchrotron data collection and processing*

After two months of storage in crystallisation trays at 16°C the crystals were transported to the European Synchrotron Radiation Facility (ESRF) at Grenoble, France.

...g and merging statistics by resolution shells.

Lower	Upper	Redund.[a]	Intens.[a]	σ(I)	I/ σ(I)	χ^2	R_{symm} (%)	No. refl.[a]
50.00	5.81	5.4	243.0	9.5	25.6	0.61	4.7	2113
5.81	4.62	5.7	196.2	11.7	16.8	0.69	8.9	2000
4.62	4.03	5.7	223.1	15.5	14.4	0.91	12.2	1993
4.03	3.66	5.1	252.2	23.6	10.7	1.47	18.1	1931
3.66	3.40	4.8	165.8	25.6	6.5	1.14	23.1	1678
3.40	3.20	5.7	108.0	17.3	6.2	0.71	25.8	1959
3.20	3.04	5.6	80.4	17.1	4.7	0.70	32.4	1949
3.04	2.91	5.5	59.4	17.0	3.5	0.68	42.7	1931
2.91	2.80	5.4	48.1	16.5	2.9	0.70	50.7	1940
2.80	2.70	5.2	31.6	13.7	2.3	0.71	61.3	1929
All shells (50-2.7)		5.4	141.7	16.5	8.6	0.82	18.3	19423

[a] Redund. = Data redundancy; Intens. = Signal intensity; No. refl. = Number of reflections

Altogether 144 diffraction images were collected, each to a resolution limit of 2 Å (Fig. 3-4). A total of 525398 diffraction spots to 2.7 Å were indexed, integrated and scaled to 105024 reflections. The symmetry-related reflections were merged, to give a total of 19423 unique reflections. The two major quality measures, I/σ (8.6), and R_{symm} (18.3%), were satisfactory for the set of reflections. In particular the I/σ ratio, although being somewhat low for expected signal-to-noise ratios in crystallographic datasets, was considerably higher than the corresponding figure for the $P2_12_12_1$ space group's systematic absences (I/σ = 0.16). Although the outermost shell (2.8-2.7 Å) had R_{symm} = 61.3%, these data were included on the basis of high completeness (99.2% – although HKL programs do not reject observations (Gewirth & Majewski, 2003); Table 3), good redundancy (5.2) and acceptable signal-to-noise (2.3) ratios. The χ^2 value (0.82) for the set of reflections is somewhat lower than unity, the ideal value, so the error model should have been adjusted during processing. However, since χ^2 is proportional to the square of the errors (σ),

even a deviation of 20% from 1.0 for χ^2 represents just a 10% adjustment in σ, which is acceptable (Gewirth & Majewski, 2003). The data collection statistics by resolution shells are shown in Table 2.

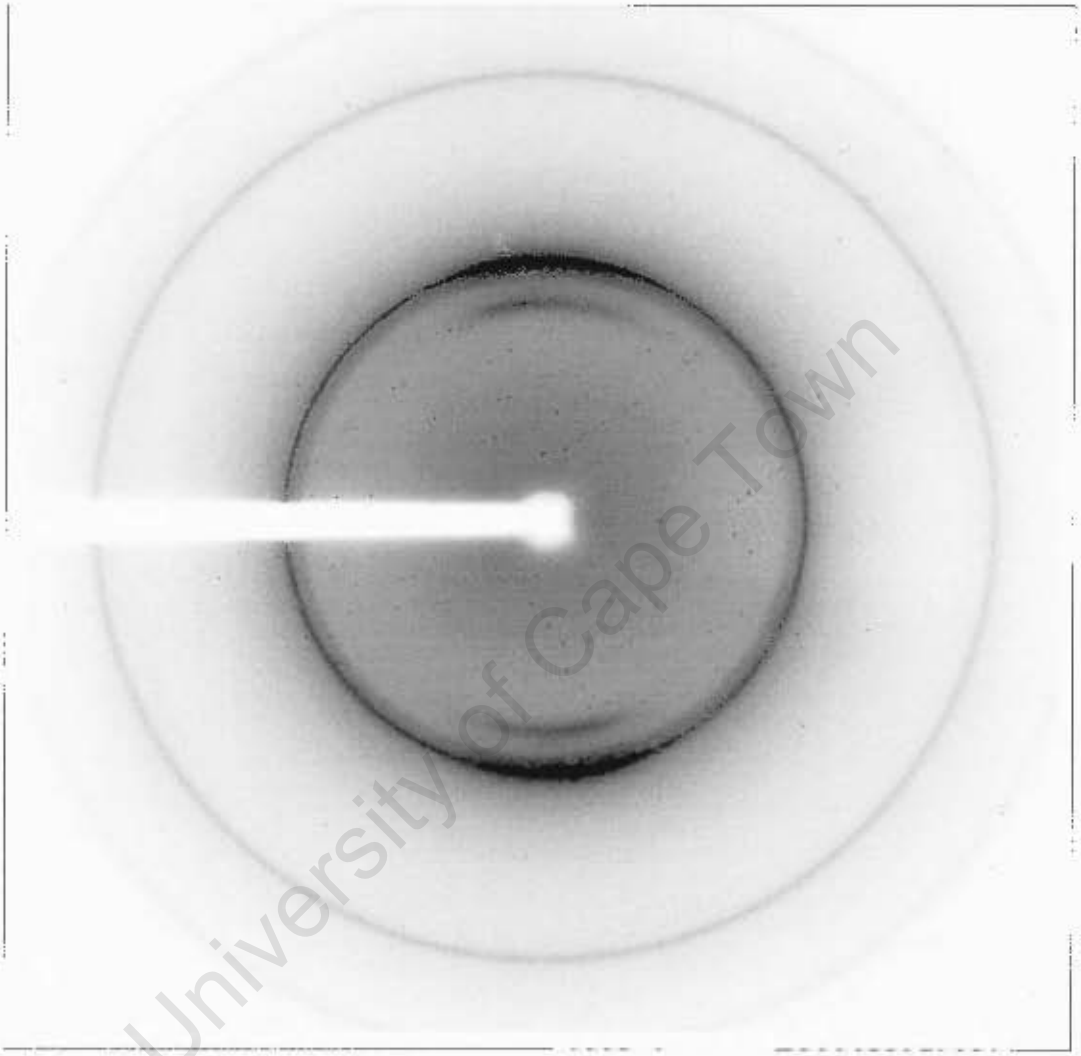

Figure 3-4. Diffraction image collected for tACE-g13–RXPA380 co-crystals at BM14-UK, ESRF.

The dark rings are due to ice and perhaps frost on the surface of the crystals (Glaeser et al., 2000). Due to the particularly dark innermost ring, the reflections collected in the range 3.6-3.4 Å were fewer, and so the redundancy of that shell was lower than all the other shells (4.8 vs average 5.4; Table 2). However, this redundancy still indicated the collection of sufficient data in the shell for data collection and subsequent structure solution.

Table 3. Crystallographic data statistics. Values in parentheses refer to the last shell (2.80–2.70 Å).

Diffraction data	Value
Unit cell (lengths in Å, angles in °)	a=59.89, b=85.15, c=135.32; α=90, β=90, γ=90
Space Group	$P2_12_12_1$
Mosaicity	0.42
Resolution range	50-2.7 Å
Total No. of reflections	105024
No. of unique reflections	19423
Completeness [a] (%)	98.2 (99.2)
Redundancy	5.4 (5.2)
I/σ	8.6 (2.3)
R_{symm} (%)	18.3 (61.3)
χ^2	0.82 (0.71)

[a]Completeness data from HKL2000 include those reflections (2044, i.e. 10.4%) which were subsequently found to have $\langle I \rangle \leq 0$. Taking these data into account, the final completeness figures were overall = 89.6%, outer shell = 81.3%.

3.4. Structure solution and refinement

Molecular replacement using EPMR v2.5 (Kissinger et al., 1999) and a native tACE-g13 structure (Watermeyer et al., 2006) as a starting model yielded a solution after just 2 cycles. The correlation coefficient was 0.693, with only one molecule in the asymmetric unit.

The first *B*-factor correction was in effect the initial assignment of *B*-factors to the atoms, and this resulted in a significant decrease in the *R*-factors (Fig. 3-6).

After the first round of refinement (comprising a given number of cycles of conjugate gradient minimisation with maximum likelihood targets – see Fig. 3-

6), the active site zinc and 2 chloride ions were located and added to the model. The sites of these ions were found at over 5σ in the $F_{obs} - F_{calc}$ Fourier difference maps. Further model building and refinement led to the addition of the glycan residues at N^{72} and N^{109}. Throughout the model building the glycan chain at N^{72} did not visibly extend beyond the first *N*-acetyl glucosamine linked to the asparagine, and eventually even this was removed from the model. At N^{109}, however, several residues were visible, and most of these were retained in the final model. Waters were also gradually added as refinement proceeded. Most of these were added after inspection of the active site and subsequent modelling of the inhibitor.

A $2F_{obs} - F_{calc}$ composite omit map was calculated in order to reduce model bias. However, this was found to be so similar to the $2F_{obs} - F_{calc}$ that it gave essentially the same information, and so its use was discontinued.

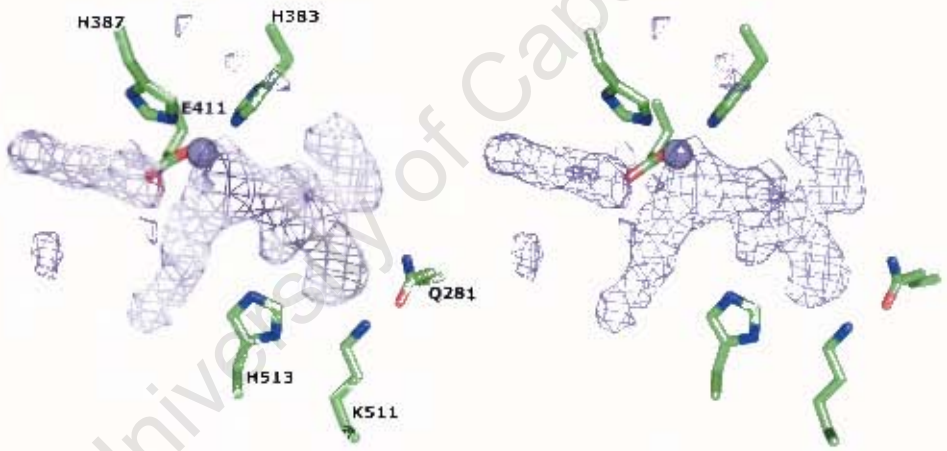

Figure 3-5. Stereo representation of active site of model with Fourier difference ($F_{obs} - F_{calc}$) map contoured at 2.5σ level, before modelling of the inhibitor. The zinc atom is shown as a sphere.

After several rounds of refinement, the $F_{obs} - F_{calc}$ map of the active site was examined at 2.5σ (Figs. 3-5, 3-6). This clearly indicated continuous density, suggesting a molecule coordinated to the zinc in an orientation similar to lisinopril and other inhibitors. A crude alignment of a model of the RXPA380-tACE complex (Fig. 3-17) with the present model and electron density map

showed that the RXPA380 molecule could account completely for the as yet unassigned density.

RXPA380 was successfully built with the correct stereochemistry and minimised using the ProDRG server (Schuttelkopf & van Aalten, 2004). This first structure was placed into the active site of the tACE-g13 model and adjusted, primarily by altering permitted torsion angles appropriately. Density for the pseudo-proline and the C-terminal tryptophan residue (particularly its side chain indole ring) could be seen very clearly between the zinc-coordinating region (occupied by the phosphinyl group) and the known C-terminus-coordinating residues K^{511}, Q^{281} and Y^{520}. On the other side (the pre-scissile bond side) the relative positions of phenyl ring and the carboxybenzyl group were easily distinguished by size, and fitted accordingly. After a round of refinement the overall position of the inhibitor was in accordance with the $2F_{obs} - F_{calc}$ electron density, although the C-terminus (particularly the tryptophan indole ring) required further attention.

Once the inhibitor model was built into the active site in a conformation that satisfied the constraints of the torsion bonds and the electron density, a final check of the model was carried out, with the addition of further water molecules and the modification of glycan residues and the side chains of other residues. In total 109 water molecules were included. A last round of restrained refinement saw the R_{cryst} and R_{free} values drop to 23.69% and 27.97%, respectively (Fig. 3-6). This improvement in phasing did not lead to any significant alterations in the density maps to allow further improvement of the model, particularly at the glycan chains or the active site. The residues 435-438 in a flexible loop and 618-623 at the C-terminus, for which continuous density could not be determined, even for the main chains, were truncated from the final model. This truncation resulted in slight increases in R_{cryst} to 23.70% and R_{free} to 28.17%, since these residues were accounting for the observed data, however insufficiently. The data refinement statistics are shown in Table 4.

Table 4. Refinement statistics.

Parameter	Value
Resolution range (outer shell)	50.0-2.7 Å (2.8-2.7 Å)
R_{cryst} (outer shell) %	23.7 (36.6)
R_{free} (outer shell) %	28.2 (40.3)
No. of protein atoms	4736
No. of solvent atoms	103
No. of inhibitor atoms	44
RMS deviations from ideality	
Bond lengths	0.009 Å
Bond angles	1.5°
Dihedral angles	20.9°
Improper angles	1.1°
Estimated coordinate error	0.37 Å
B-factors (Å^2)	
Overall mean *B*-factor	29.6
Protein main chain *B*-factor	29.8
Protein side chain *B*-factor	31.3
Solvent atoms	21.2
Inhibitor atoms	23.2
Zinc atom	13.9
Chloride atoms (CL1, CL2)	12.4, 18.4
Ramachandran analysis	
Residues in favoured regions (%)	533 (93.5)
Residues in allowed regions (%)	36 (6.3)
Residues in disallowed regions (%)	1 (0.2)

$R_{cryst} = \Sigma_h \{|F_{obs}| - |F_{calc}|\} / \Sigma_h |F_{obs}|$, where F_{obs} and F_{calc} are the observed and calculated structure factor amplitudes of the reflection h.

$R_{free} = \Sigma_h \{|F_{obs}| - |F_{calc}|\} / \Sigma_h |F_{obs}|$, where F_{obs} and F_{calc} are as above, for a test set of 3.7% of the reflections that were unused in refinement.

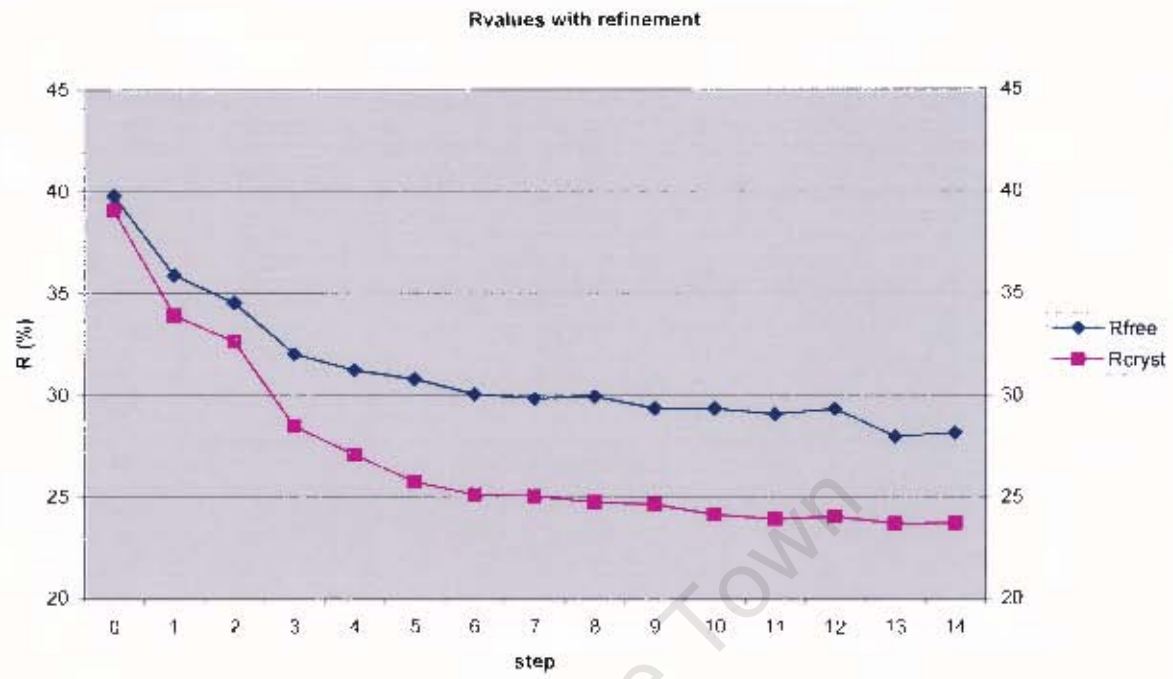

Step	Action
1	*B*-factor correction
2	10× restrained refinement
3	Ions added; Group *B*-factor refinement
4	Model-build, 12× restrained refinement
5	Waters in, model-build, 20× restrained refinement
6	Model inspection, 32× restrained refinement 8× *B*-factor refinement
7	Waters added, 4× restrained refinement, 7× *B*-factor refinement
8	Inhibitor added. 12× restrained refinement
9	Inhibitor position improved; 16× restrained refinement. 6× *B*-factor refinement
10	Inhibitor tryptophan positioned; 24× restrained refinement
11	Waters in, 2 glycans out; 29× restrained refinement
12	H, N, Q flips rotamer outliers adjusted 13× restrained refinement, 3× *B*-factor refinement
13	Waters in, g1 glycan out, model inspection: 27× restrained refinement, 5× *B*-factor refinement
14	Disordered regions (434-437, 618-623) removed

Figure 3-6. Progression of *R*-factors with model building and refinement, with appended table outlining refinement action.

The side chains of three N, nine Q and three H amino acid residues were "flipped" by the MolProbity server (Davis et al., 2004), in order to improve the probable hydrogen-bonding network of the molecule. These flipped N residues did not include N^{72} or N^{109}, as these are the sites of glycosylation, and have fixed side chain orientations.

Table 5. Comparison of unit cell dimensions of tACE structures determined to date.

Structure (pdb code)	*a* (Å)	*b* (Å)	*c* (Å)	Unit cell volume (Å^3)
Native tACE (1o8a)	56.62	85.06	133.79	644345.8
tACE–lisinopril (1o86)	56.47	84.90	133.99	642388.7
tACE–captopril (1uzf)	56.65	84.90	133.50	642079.6
tACE–enalaprilat (1uze)	56.72	85.35	133.73	647393.9
tACE-g13 [a]	59.81	84.90	135.99	690539.4
tACE-g13–RXPA380	59.89	85.15	135.32	690060.2

[a] J.M. Watermeyer (2004).

3.5. Structure validation

MolProbity C_β and rotamer plot checks revealed no structural anomalies requiring urgent attention (Davis et al., 2004). Ramachandran plots and other analyses indicated satisfactory geometry. A few outliers flagged in the MolProbity-generated Ramachandran plot were checked and adjusted accordingly. These included A^{354}, whose carbonyl oxygen has been shown to coordinate the lysyl amine nitrogen in the tACE-lisinopril complex (Natesh et al., 2003).

The final structure (after the truncations) was not minimised because the changes to which the penultimate model was subjected were collectively minor, and the R_{free} value, in remaining constant or increasing with more cycles of minimisation, indicated that over-refinement was a distinct possibility.

Final Ramachandran plots from MolProbity (Davis et al., 2004) and PROCHECK (Laskowski et al., 1993) for this final adjusted model indicated that almost all residues had satisfactory *phi* and *psi* angles (Fig. 3-7, Table 4). The only non-glycine exception was A^{129}, which is marginally an outlier according to MolProbity. This can be attributed to the fact that this residue follows a proline in sequence, and occurs effectively at the junction between loop and α-helix 4.

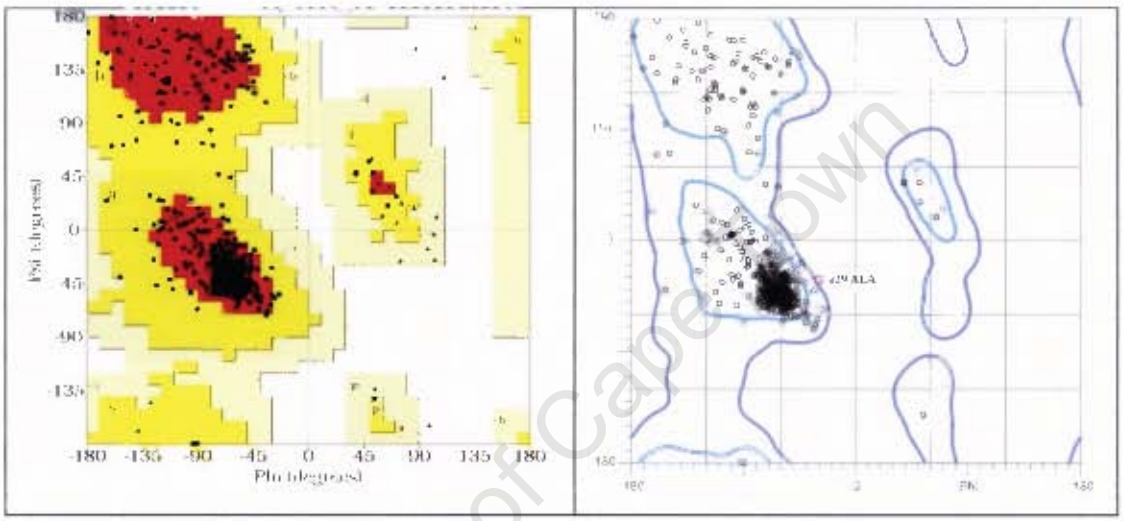

Figure 3-7. Ramachandran plots. Left: PROCHECK Ramachandran plot of final model. Only a few glycine residues (represented by triangles), are to be found in the disallowed regions, shown in white. Right: MolProbity Ramachandran plot of final model, excluding glycine and proline residues.

3.6. Structural analysis

3.6.1. Overall structure of tACE-g13–RXPA380 complex

Like other tACE structures, the present structure reveals a predominantly helical protein, elliptical in shape and containing a buried active site between two sub-domains. The tACE-g13 unit cell is marginally larger than the tACEΔ36NJ, from the dimensions of both the native structure and this ligand-bound structure (Table 5).

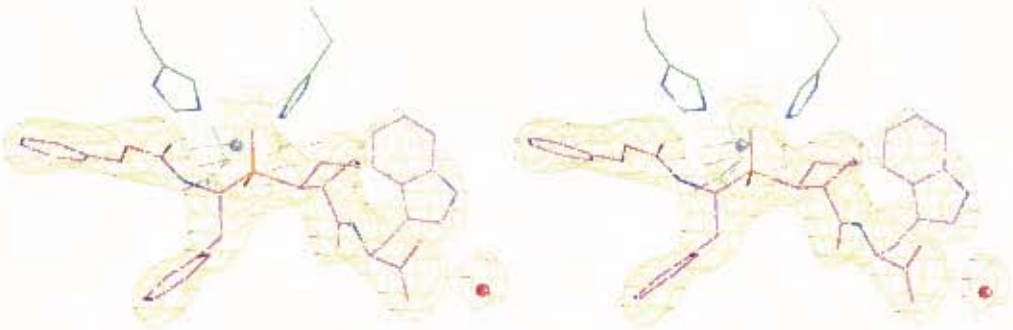

Figure 3-8. Stereo view of final modelled position of RXPA380 (purple carbons, phosphorus in orange) in tACE-g13 active site and its fit with experimental density map. The catalytic triad (H^{383}, H^{387}, E^{411}) is shown in green lines. The zinc ion and a C-terminal carboxylate-coordinating water are shown as metallic blue and red spheres, respectively. Density map is $2F_{obs} - F_{calc}$ contoured at 1.3σ.

Both domains contribute residues to the active site (Natesh et al., 2003). The alignment of tACE-g13–RXPA380 with the other structures reveals almost no difference between them (r.m.s.d. values = 0.24 Å [tACE–lisinopril], 0.26 Å [tACE–enalaprilat], 0.26 Å [tACE –captopril]; Fig. 3-9; Fig. 3-14).

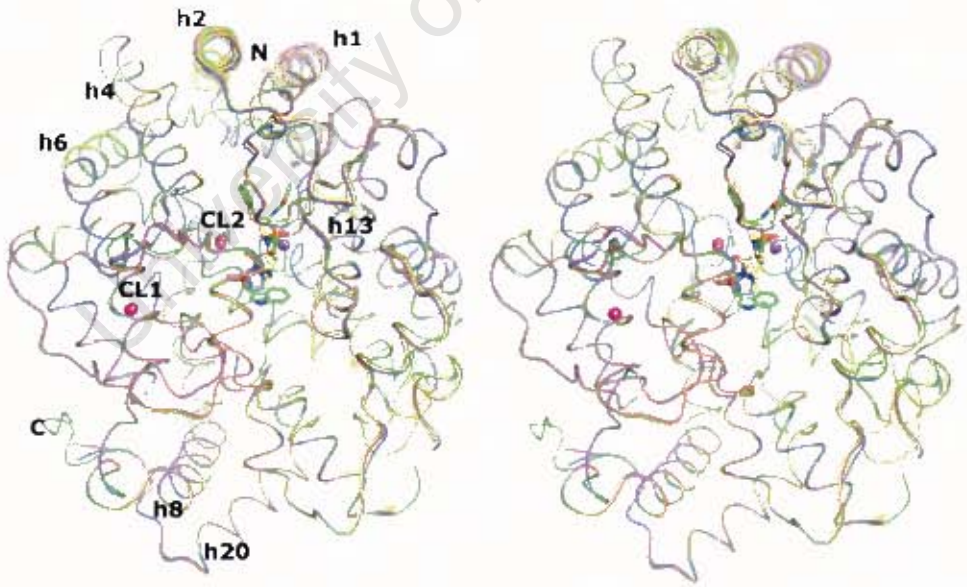

Figure 3-9. Stereo diagram of all-C_α alignment of tACE–inhibitor complexes: tACEΔ36NJ–enalapril (1uze, purple), tACEΔ36NJ–captopril (1uzf, blue), tACEΔ36NJ–lisinopril (1o86, yellow) and tACE-g13–RXPA380 (green). Inhibitors are shown as sticks in corresponding colours. The zinc and chloride ions are shown as purple and hot pink spheres, respectively.

Glycosylation and chloride binding

Testis ACE-g13 has intact glycosylation sequons only (g3). As with the previously determined native tACE-g13, the extent of glycosylation that can be correlated with continuous electron density from difference or omit maps is greater at N^{109} (Fig. 3-10). In this case, no density could be interpreted even for the ring portion of the first *N*-acetyl glucosamine residue linked to N^{72}.

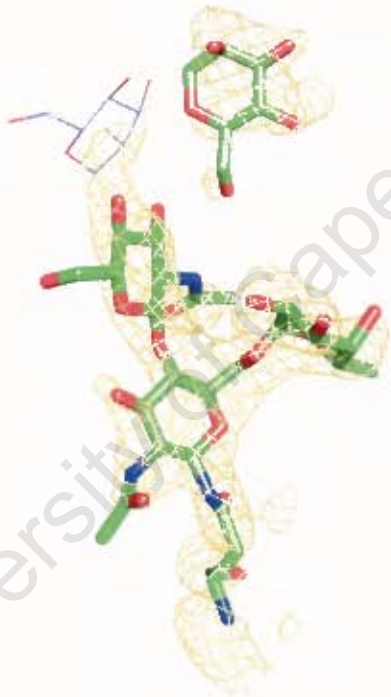

Figure 3-10. Glycosylation of tACE-g13–RXPA380 at N109, residues shown as sticks. Density map is $2F_{obs} - F_{calc}$ at 1.2σ. The penultimate residue (mannose), for which sufficient difference density could not be discerned, is rendered as lines.

The glycosylation at N^{109} appears to be more extensive than that which occurs at N^{72} in tACE-g13 (Watermeyer et al., 2006), at least with respect to those glycan residues whose occupancy is sufficiently high and temperature

factors sufficiently low to allow their incorporation into the model. The N72 glycosylation site has been shown to occupy a larger water channel than that taken up by N^{109}, which could explain the greater degree of order observed at the N^{109} site. This sole glycosylation site, along with the rest of the tACE surface, is sufficient for intermolecular contacts that facilitate crystallisation (Watermeyer et al., 2006).

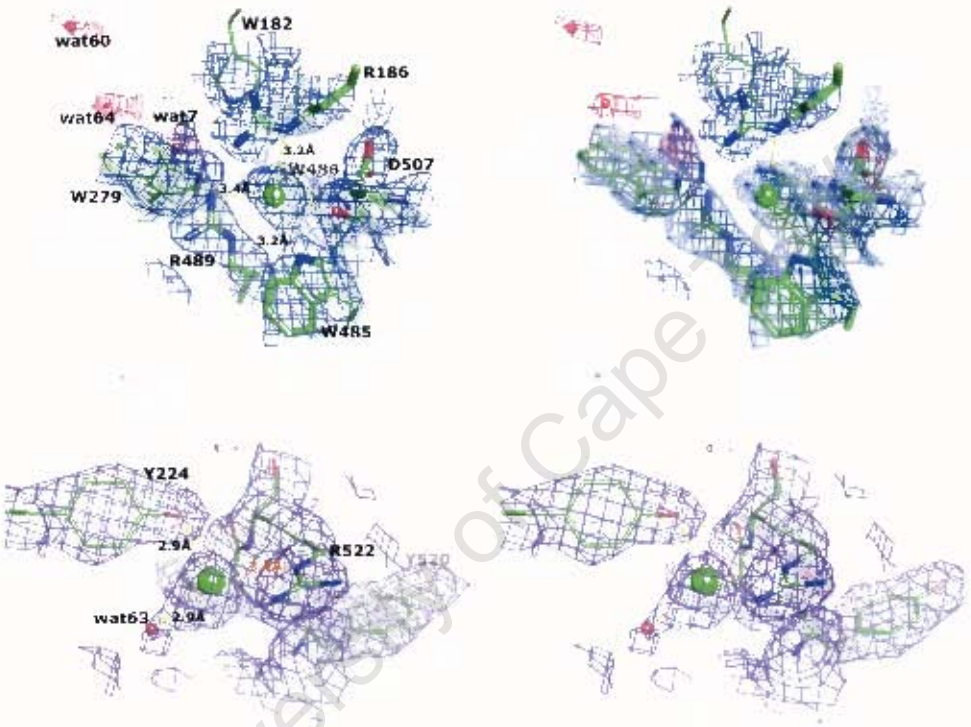

Figure 3-11. Chloride binding sites of tACE-g13–RXPA380. A. Cl^1 site with water channel. The tryptophan residues making up the hydrophobic shell are shown as lines (except the chloride ligand W^{485}). $2F_{obs} - F_{calc}$ density maps are contoured at 1.2σ.

The chloride sites (Fig. 3-11) were easily discernible, as they were located (together with the zinc ion) as peaks above 5σ in a Fourier difference map. The *B*-factors were refined to 12.4 $Å^2$ and 18.4 $Å^2$ for Cl^1 and Cl^2, respectively. The binding site of Cl^1 occurs within a hydrophobic shell of four tryptophan residues ($W^{182, 279, 485, 486}$), one of which (W^{485}) is also a chloride ligand. In addition, two arginine residues, R^{186} and R^{489}, coordinate the chloride from 3.2 Å and 3.4 Å, respectively. The fourth ligand, a water

molecule, could not be located with certainty at this resolution, although there is a water molecule 5 Å away that seems to form the end of a system of water residues leading to the channel.

At Cl^2, the three ligands of the anion were side chains of R^{522} (N_ε atom) and Y^{224} (O_η atom). The presence of a water channel from the milieu into the Cl^2 site has been postulated by Tzakos and colleagues (2003), but strong evidence for this was not observed at the site.

3.6.3. Binding of RXPA380 to tACE-g13

3.6.3.1. Overall

RXPA380 has been shown to bind to the C-domain of ACE with a K_i of 3 nM, comparable with the most tightly binding inhibitors of ACE (Wei et al., 1992; Georgiadis et al., 2004). This inhibitor binds to tACE-g13 in an extended conformation with its central phosphinate group coordinated to the catalytic zinc (Fig. 3-8). Three residues, K^{511}, Q^{281} and Y^{520}, coordinate and stabilise the C-terminal carboxylate from 2.6, 3.0 and 3.8 Å, respectively. A water molecule, wat11, appears to be coordinated to both oxygens of the carboxylate. The zinc atom is penta-coordinated (T_5, trigonal bipyramidal configuration) to the catalytic triad and the two phosphinyl oxygens (Fig. 3-12). The two phosphinyl oxygen–zinc bonds are distinctly different in length, at 2.56 Å (Zn–O^{AT}) and 1.84 Å (Zn–O^{BL}), as is the case with other phosphinate-metalloprotease complexes. In the bidentate coordination one of the bonds is usually longer than the other, on average 2.54 Å and 2.14 Å in the case of carboxypeptidase A- and leucine aminopeptidase-phosphonate complexes (Kim & Lipscomb, 1990; Strater & Lipscomb, 1995; Alberts et al., 1998). Stromelysin-3, or matrix metalloprotease 11, also has unequal bidentate coordination phosphinate bonds in its complex with a phosphinic inhibitor (means of 2.89 Å and 2.33 Å for the two P–O bonds in the six molecules of the asymmetric unit) (Gall et al., 2001). A general feature of the binding site of RXPA380 to tACE-g13 is the considerable space between sub-site residues and the inhibitor. Only 12 atoms (from 8 amino acid residues, and including zinc and a water) are found within 3 Å of any inhibitor atoms.

This is comparable with 10 atoms (of 6 amino acids, plus three waters and zinc) within 3 Å of lisinopril in 1o86, despite the fact that RXPA380 (44 non-H atoms) is a considerably larger molecule than lisinopril (29 non-H atoms).

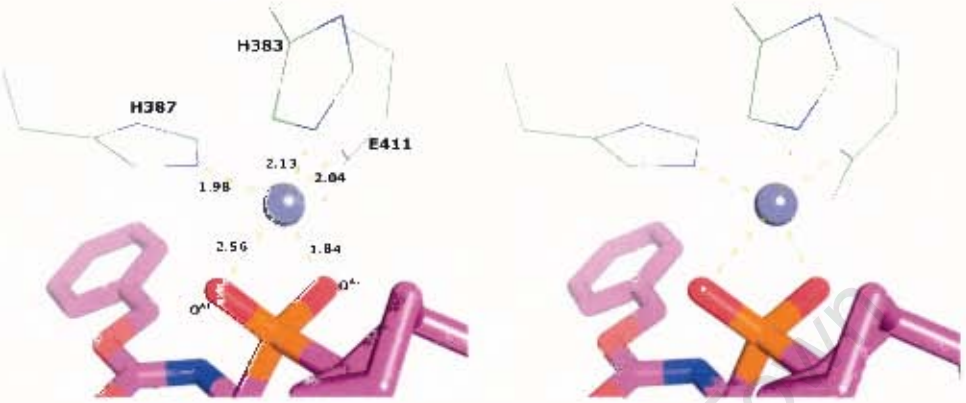

Figure 3-12. Stereo view of catalytic zinc penta-coordination in the active site of tACE-g13 complexed with RXPA380. Distances between zinc and coordinating atoms shown in Angströms.

3.6.3.2. S2 sub-site

Positioning of an inhibitor sub-group at the S2 position has not been previously observed in tACE–inhibitor complexes, as the inhibitors were all Type II or Type III inhibitors (Fig. 1-4). The benzene ring has hydrophobic interactions with H^{410} and F^{391}, the only side chains that are within 4 A of it (Fig. 3-13). A hydrogen bond between the amine nitrogen of A^{356} and the carbonyl oxygen of the Cbz group (2.46 Å) likely prevents any flexible motion of the Cbz moiety, keeping it fixed in the side pocket (Fig. 3-13).

3.6.3.3. S1 sub-site

The hydrophobic phenyl ring in the P1 position interacts with the C_β of S^{355} proximally, and with F^{512} and V^{518} distal to the P2 and zinc-binding groups. Nothing else in the S1 pocket is close enough to make significant interactions with the ring. All of the previously determined ACE-inhibitor complexes (with the exception of tACE–captopril, 1uzf) have this phenyl ring, also referred to

as a phenylpropyl group, and it occurs in essentially the same orientation in all of them (Fig. 1-7, 3-14).

Figure 3-13. S2 and S1 residues of tACE-g13–RXPA380. Residue side chains (except A^{354}, S^{355} and A^{356}) have been omitted for clarity.

3.6.3.4. S1' sub-site

This sub-site is occupied by a pseudo-proline moiety, i.e. a proline with the amine nitrogen substituted by a carbon, described as the C_γ carbon. This carbon is in the *R* stereo-configuration, in contrast with the adjacent C_α carbon, which is *S*, as would be expected in proline. An alignment of active site residues from 1o86 and the tACE-g13 – RXPA380 complex confirms the prediction that the *R*-configuration of the C_γ carbon, together with the essential *S*-configuration at the P1' C_α (Cushman et al., 1977), allows the prolyl ring to adopt the same directional conformation as the lysyl chain in tACE lisinopril (Georgiadis et al., 2004) (Fig. 3-14). Notably, the carbonyl oxygen of A^{354} is marginally displaced away from the inhibitor (relative to the corresponding C–O bond in tACE–lisinopril), probably due to the presence of a carbon atom (C_γ) in place of the H-bond donor. In tACE–lisinopril this carbonyl oxygen forms a hydrogen bond with the main chain N.

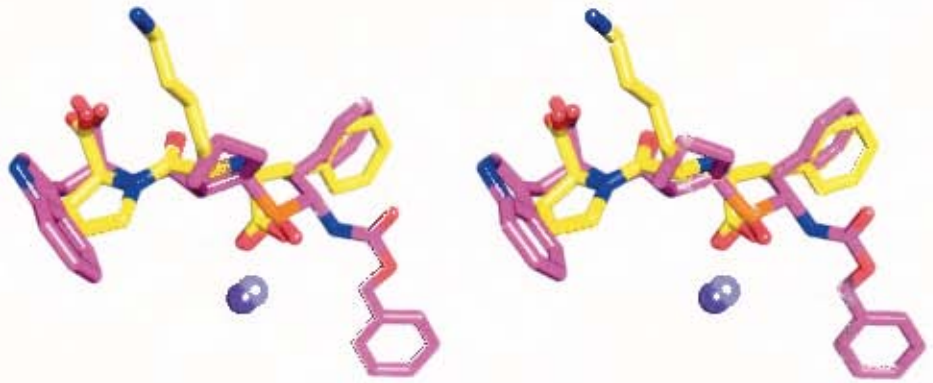

Figure 3-14. Stereo view of Cα alignment of tACEΔ36NJ–lisinopril (yellow) and tACE-g13–RXPA380 (purple, r.m.s.d. = 0.24 Å) produces substantial correspondence between inhibitor residues. Enalapril and captopril are essentially fully superimposable over lisinopril. The overlapping zinc cations are shown in mauve (that of tACE-g13–RXPA380 is lighter in shade).

3.6.3.5. S2' sub-site

The S2' pocket of tACE-g13–RXPA380 complex is a large binding pocket (Fig. 3-15). There are 10 residues within 5 Å of the tryptophan side chain (Table 6). In addition, there are two water molecules, wat11 that is coordinated to the C-terminal carboxylate, and wat13, which mediates the interaction between the tryptophan N_ε and the E^{376} side chain.

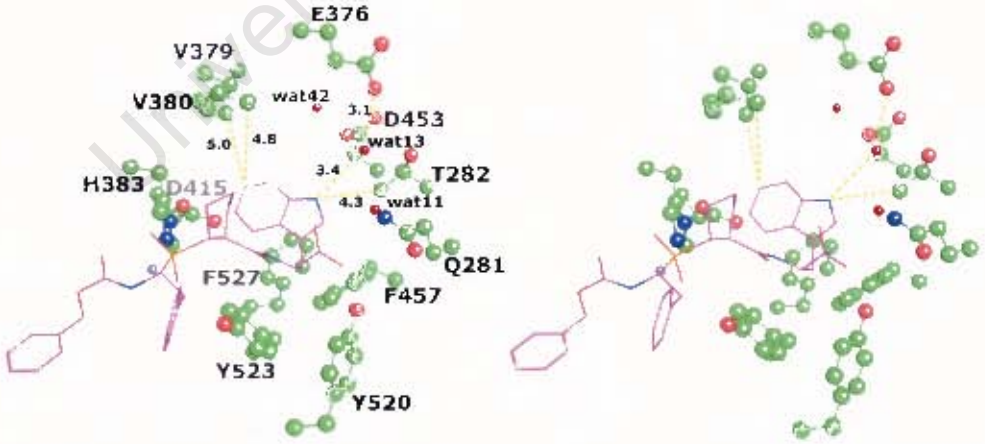

Figure 3-15. Stereo view of tACE-g13 S2' pocket containing RXPA380 tryptophan residue. The 10 amino acid residues within 5 Å of the P2' tryptophan as well as E^{376} and D^{453} are shown in ball-and-stick notation. Water molecules are shown as maroon spheres. Selected distances (in Å) between the tryptophan and tACE-g13 residues are labelled.

D^{453}, whose side chain is further than 6 Å from RXPA380, forms a hydrogen bond with a water molecule in the upper recesses of the S2' pocket; this interaction is likely to keep the side chain in an angled conformation, away from the P2' tryptophan.

3.6.4. tACE-g13–RXPA380 vs ACE N-domain sub-sites

A C_α alignment (544 atoms, r.m.s.d. = 0.77 Å) of tACEg-13–RXPA380 and the ACE N-domain complexed with lisinopril (pdb code 2c6n, A chain) allows a comparison of the sub-sites of the two domains (Fig. 3-16).

The major difference in the S2 pocket is the presence of tyrosine in place of F^{391} of tACE. This may provide opportunity for a weak (due to length: 3.57 Å) hydrogen bond between the tyrosine hydroxyl and carboxy group of Cbz. At P1 the slight shift of the phenylpropyl ring is consistent with the presence of a polar threonine residue in place of V^{518} (Fig. 3-16). Both these substitutions are consistent with the selectivity of the N-domain for RXP407, which has a N-terminal aspartate residue.

The differences between N- and C-domain S1' pockets have been described previously (Natesh et al., 2003; Corradi et al., 2006). One noteworthy point is that the alignment of the A chain of N-domain–lisinopril reveals particularly close contact between the carbonyl oxygen of A^{332} (equivalent to A^{354} in tACE) and the C_δ of the pseudo-proline (2.0 Å; *cf.* 2.9 Å in tACE-g13–RXPA380). In the lisinopril complexes this oxygen forms a hydrogen bond contact with the lysyl amine nitrogen. The variance in length of this H-bond between the domains (2.6 Å N-domain–lisinopril vs 2.9 Å tACE–lisinopril), together with the clash already mentioned, suggest that there may be conformational restraints on the N-domain that prevent it from easily accommodating the constrained pseudo-proline.

The S2' pocket comparisons reveal several differences. The replacement of V^{379} and V^{380} with S^{357} and T^{358} in the N-domain increases the polar nature of the pocket, and reduces the possibility of stabilising van der Waals' interactions with the indole ring. D^{453} in the C-domain is replaced by a glutamate, whose side chain faces away from the P2' residue, precluding any reorientation occurs at the site of another conservative substitution. In tACE wat13 is H-bonded to both E^{376} and the indole nitrogen. This connectivity is not possible in N-domain due to replacement of the E by D^{354}. Not only is this side chain shorter than that of glutamate, but it also faces into the protein, well away from the inhibitor. (It must be noted, however, that both chains of the N-domain structure contained no modelled water residues in the region of the P2' pocket, most likely due to lower resolution of 3.0 Å) Taken together, these changes allow the S2' pocket to be considered as the major determinant sub-site in the difference in binding affinity of RXPA380 to the C- and N-domains.

Analysis of the internal pockets in tACE-g13–RXPA380 and the N-domain–lisinopril structure (pdb code 2c6n, A chain) uncovers substantial differences in the overall conformation of the S1' and S2' pockets. CASTp analysis (Binkowski et al., 2003) revealed that the N-domain S1' and S2' pockets are effectively contiguous when probed with a 2.5 Å-radius probe, forming a large cavity of volume 1152 $Å^3$. By contrast, although the pocket comprising the tACE-g13 S2' residues also incorporates a number of the S1' residues, at 857 $Å^3$ this pocket is much smaller than that found in the N-domain. This difference in volumes and the substitution of S2' C-domain residues by smaller residues in the N-domain ($T^{282}S$, $V^{379}S$, $V^{380}T$, $E^{376}D$), together point to the availability of fewer residues in the N-domain for interaction with the inhibitor.

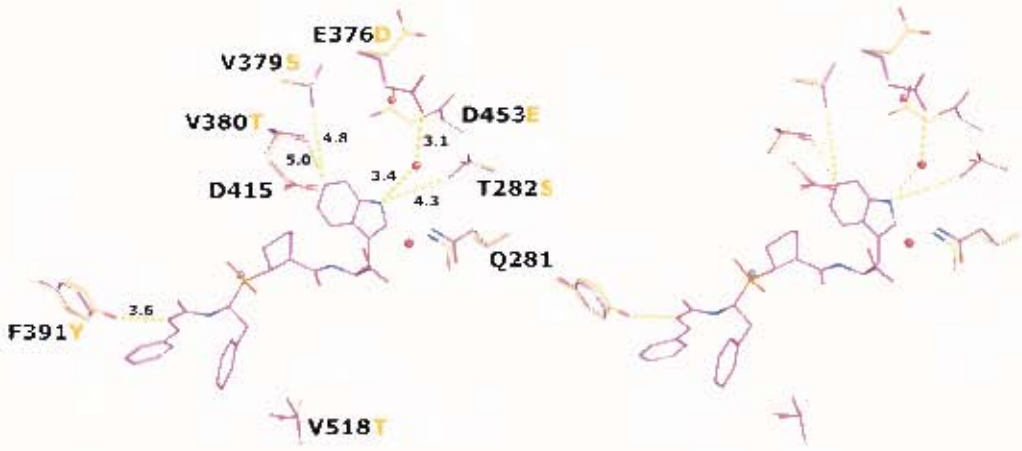

Figure 3-16. Stereo view comparison of tACE-g13 (≡C-domain) (purple) and ACE N-domain (gold) sub-site residues, with particular emphasis on S2' pocket, and with RXPA380 in the active site. tACE numbering is used, sites where N-domain residues differ are indicated with gold letters. Selected distances (in Å) indicated with yellow dotted lines. All water molecules (red spheres) are from tACE-g13–RXPA380 structure.

The overall stabilisation of the RXPA380 molecule by means of interactions at the S2' pocket and the rigid conformation maintained due to the *R-S* configuration of the pseudo-proline together seem to make the difference with respect to selectivity. Compound 9, an RXPA380 analogue in which pseudo-proline and tryptophan are replaced by pseudo-alanine and alanine, has identical K_i values for the N- and C-domains. Indeed, the measured K_i values (0.8 nM in each case) were lower than that of RXPA380 with C-domain (Georgiadis et al., 2004), suggesting that the sub-site interactions do not necessarily enhance binding, but merely provide a means for discrimination between the two domains. It may be speculated that the S2' pocket is sufficiently large to allow binding of various sizable P2' constituents. For example, compound 11 is another RXPA380 analogue, which has pseudo-arginine in P2' and is otherwise identical to RXPA380. It binds C-domain with K_i = 9 nM which is quite similar to that of RXPA380 (Georgiadis et al., 2004). But the interactions of this group with the S2' pocket of N-domain appear not to be as non-complementary as those of the indole ring, since K_i = 200 nM for the N-domain. Therefore differences in the S2' pocket distinguish the two domains without necessarily resulting in tighter binding.

3.6.5. *Comparison of experimentally determined tACE-RXPA380 and modelling predictions*

In light of the difficulties faced in terms of obtaining co-crystals of tACE-g13 and RXPA380, the *in silico* docking and modelling of tACE and RXPA380 was undertaken concurrently. In the event of the successful co-crystallisation of the complex and subsequent structure solution and refinement, it is worthwhile to compare the experimental structure with the structure predicted from *in silico* modelling.

The energy-minimised tACE–RXPA380 molecular model (RXPA380MM) was found to have more residues found in the generously allowed/outlier regions of the Ramachandran plot. This was not considered to be a serious mark against drawing conclusions about the possible binding of inhibitors at the active site of the models. The minimisation algorithm allows the free movement of atoms to attain the most overall energetically stable state, and no constraint was imposed on *phi* and *psi* angles during the iterative minimisations. Nevertheless, the Ramachandran plot of the residues of the active site (residues wholly or partially within 5 Å of the inhibitor) was preferentially examined carefully in order to ensure that no gross distortions of the active site region were overlooked.

The C_α alignment of tACE-g13–RXPA380 and RXPA380MM revealed an r.m.s.d. of 1.55 Å. Alignment of residues within 5 Å of the tACE-g13–RXPA380 gave an r.m.s.d. of 1.15 Å. Immediately evident in this alignment was the general correspondence of all atoms with the clear exception of the inhibitor's P2 Cbz group. The pseudo-proline rings were also not so well aligned, especially at the C_ε carbon. The P2' tryptophan side chain and the P1 phenylpropyl group aligned particularly well. The all-inhibitor alignment (r.m.s.d. = 1.07 Å) and the same alignment excluding the Cbz group beyond the amine nitrogen (r.m.s.d. = 0.61 Å) indicate the level of similarity between the predicted orientation and that of the experimental structure (Fig. 3-17).

Table 6. Predictions of tACE–RXPA380 conformation at S2' pocket compared with experimentally determined structure. Distances of 12 residues (in bold) predicted to be within 5 Å of RXPA380 (Georgiadis et al., 2004). Tryptophan – S2' side chain distances are measured in current modelled structure (RXPA380MM) and experimental structure (tACE-g13–RXPA380). Additional residues within 5 Å are included. Shortest inter-atomic distance between residue and tryptophan side chain is given in Ångströms.

Residues [a]	RXPA380MM prediction	tACE-g13–RXPA380
Q^{281}	3.5 $N_{\varepsilon 2} - C_{\delta 1}$	3.1 $N_{\varepsilon 2} - C_{\delta 1}$
T^{282}	3.5 $C_{\gamma 2} - N_{\varepsilon 1}$	4.3 $C_{\gamma 2} - N_{\varepsilon 1}$
E^{376}	*6.5 $O_{\varepsilon 2} - N_{\varepsilon 1}$*	*6.1 $O_{\varepsilon 2} - N_{\varepsilon 1}$*
V^{379}	4.3 $C_{\gamma 1} - C_{\zeta 2}$	4.8 $C_{\gamma 1} - C_{\eta 2}$
V^{380}	4.1 $C_{\gamma 2} - C_{\zeta 2}$	4.8 $C_{\gamma 2} - C_{\zeta 2}$
D^{415}	4. 7 $O_{\delta 2} - C_{\zeta 3}$	3.7 $O_{\delta 1} - C_{\zeta 3}$
D^{453}	*5.3 $O_{\delta 1} - C_{\zeta 2}$*	*6.2 $O_{\delta 2} - N_{\varepsilon 1}$*
F^{457}	3.1 $C_{\zeta} - C_{\beta}$	3.5 $C_{\zeta} - C_{\beta}$
F^{460}	*6.5 $C_{\varepsilon 2} - C_{\delta 1}$*	*6.5 $C_{\varepsilon 2} - C_{\beta}$*
Y^{520}	3.8 $O_{\eta} - C_{\beta}$	3.3 $O_{\eta} - C_{\beta}$
Y^{523}	3.8 $C_{\delta 2} - C_{\beta}$	3.7 $C_{\delta 2} - C_{\beta}$
F^{527}	3.9 $C_{\zeta} - C_{\eta 2}$	4.5 $C_{\varepsilon 1} - C_{\varepsilon 3}$
H^{383}	3.8 $C_{\gamma} - C_{\zeta 3}$	3.7 $C_{\gamma} - C_{\zeta 3}$
Wat11	–	4.5 $O - C_{\delta 1}$
Wat13	–	3.4 $O - N_{\varepsilon 1}$

[a] residues in **bold** are S2' residues from Georgiadis *et al.* (2004). In each column the first-named atom is from the residue side chain, and the second atom is of the RXPA380 tryptophan residue. The *italicised* residues are those more than 5 Å from the RXPA380 tryptophan.

Equally significant are the discrepancies between the positions of important residues in the P2' pocket. The prediction underestimates the distances between valines 379 and 380 and the tryptophan residue by 0.5 and 0.7 Å, respectively (Table 6). The predicted positions of T^{282}, F^{457}, and F^{527} also collectively reduce the volume of the P2' pocket (Fig. 3-17, Table 6).

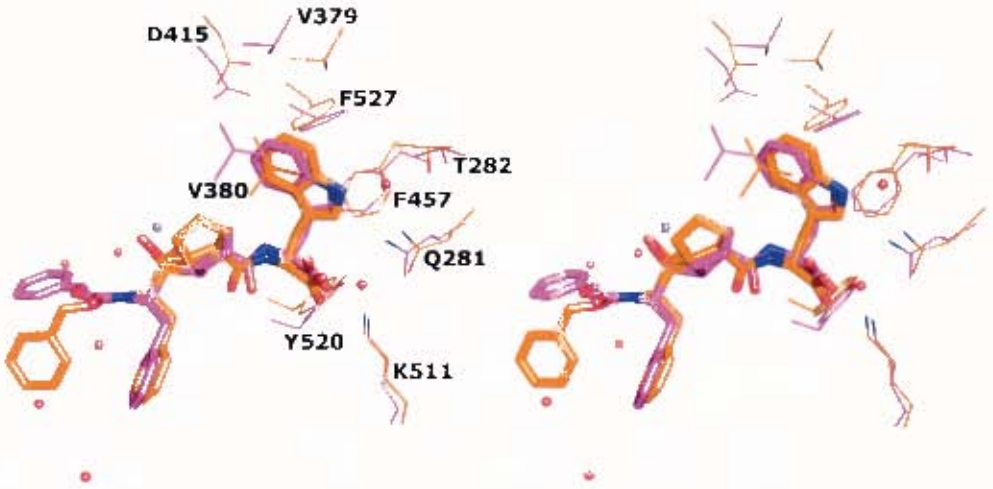

Figure 3-17. Stereoscopic view of alignment of Insight II-generated tACE–RXPA380 model (orange) and experimentally determined tACE-g13–RXPA380 (purple). 32 inhibitor atoms (the Cbz group was excluded) were aligned with r.m.s.d. = 0.61 Å. All water molecules (red spheres) are from the tACE-g13–RXPA380 structure.

The consistent valence force field (CVFF) has its limitations with regard to its applicability to systems with bonded metals. It is a classical force field, and has been parameterised for amino acids, proteins and small molecules. As described in Materials and Methods, this force field is not parameterised to recognise zinc and therefore the solution around this was to use magnesium instead. However, the parameters assigned to the metal as a result are automatically generated, and thus not fully appropriate. The extensible systematic force field (ESFF) is a more appropriate force field to use, as it both recognises zinc explicitly and relies on atomic parameters that are combined with empirically derived rules, which are used to generate force field parameters.

Another criticism of the RXPA380MM lies in the method of generation of an average structure. The use of an average conformation may result in a highly distorted starting model for minimisation, and ultimately a distorted final model, particularly if the minimisation is not allowed to go on to convergence (as was the case) (Dr Jodi Shaulsky, personal communication).

These criticisms aside, the model-generated structure bore substantial similarity to the experimentally determined structure. The previously unseen P2 group is the notable exception, as it was not in the correct position. It appears that the orientation of this group may have been much closer to that of the tACE-g13–RXPA380 complex if the methylphenyl group had been attached to the other oxygen of the carboxy group during the building of the inhibitor. (But there was no obvious reason to choose one oxygen over the other.) Put another way, it may be that the modelling allows too much flexibility in this region where it appears that the spatial constraints imposed by the protein are reduced. The crystal structure *B*-factors of the inhibitor atoms (all below 30 $Å^2$) give no evidence of such a reduction, and therefore do not support much flexibility for the P2 group.

In any case, optimisation of the protocol, particularly in terms of the use of the best force field, ESFF, may allow for the confident generation of more putative ACE–inhibitor complexes that give insight to domain-selective binding without the difficulties attendant to co-crystallisation.

4. CONCLUSIONS

4.1. Protein expression, purification and crystallisation

The expression and purification of the glycosylation mutant tACE-g13 has proved to be a solid foundation upon which to extend structural investigations of angiotensin-converting enzyme in our laboratory. Completed and ongoing work has seen the stable expression of tACE-g13 in Chinese hamster ovary cells, the crystallisation and structure determination of native tACE-g13 (Gordon et al., 2003; Watermeyer et al., 2006), and now the co-crystallisation of tACE-g13 with the potent C-domain-selective inhibitor RXPA380. The co-crystallisation conditions were essentially identical to those for native enzyme crystallisation, with the addition of a 4-fold molar excess of inhibitor yielding co-crystals.

4.2. Data collection, structure solution, refinement and analysis

The successful use of the protein crystallography beamline BM14-UK at the ESRF in Grenoble, France, is a milestone for South African structural biology. The structure of tACE-g13–RXPA380 has been solved to 2.7 Å resolution by molecular replacement, and refined in CNS.

The structure of tACE-g13–RXPA380 represents the structure determination of an ACE–type I inhibitor complex; that is, of an inhibitor with a P2 constituent group. All published structure complexes are of ACE with type II or type III inhibitors. This P2 group occupies a large pocket and interacts hydrophobically with nearby residues.

The P1 phenylpropyl group and P1' pseudoproline groups are in close alignment to the corresponding P1 phenylpropyl and P1' lysyl groups of the tACE–lisinopril complex.

The P2' group has been considered the determinant of C-domain selectivity. The interactions revealed by the three-dimensional structure firmly support this hypothesis, particularly in view of the interactions of hydrophobic V^{379} and V^{380} with the tryptophan indole ring, and of the water molecule that is H-bonded to both the indole nitrogen and E^{376}. The shorter aspartate residue in the N-domain replaces this glutamate, and so the interaction is in all likelihood lost.

4.3. Comparison of modelled tACE-g13–RXPA380 predictions with experimental structure

The modelling of the interaction between tACE and RXPA380 provided an opportunity to assess the quality of the predicted model with respect to the experimentally determined structure. The INSIGHT II-generated model agreed well with the experimental structure, with the explainable exception of the P2 group. It appears that the inversion of the carboxyl moiety of the P2 group could not be corrected during the INSIGHT II dynamics run.

Thus the structure has revealed a binding mode very similar to predictions made by the synthetic chemists responsible for RXPA380 (Georgiadis et al., 2004), and in modelling experiments carried out locally. These results suggest that one can look with confidence upon modelling predictions, although there were a number of methodological issues to consider. The appropriate choice of force field was the most important of these.

4.4. Directions for future work

Now that the hypothesis that the S2' pocket interactions are the major driver of selectivity has been confirmed, it remains to be seen just how the RXPA380 molecule interacts with the N-domain. In conjunction with such putative crystallographic work, it would also be useful to attempt co-crystallisation of the N- and C-domains with the other phosphinate inhibitors

synthesised by Dive and colleagues (Dive et al., 1999; Dive et al., 2004; Georgiadis et al., 2004). The data they have already collected on inhibition, together with the current study, point to the likelihood that although C-domain selectivity can be gained or lost by a P2' change alone, the selective binding of an inhibitor is due to subtler cumulative effects at the binding site and possibly beyond that. The dynamic aspects of enzyme catalysis have historically proven difficult to elucidate. For example, nuclear magnetic resonance spectroscopy studies (Galanis et al., 2003) have not yet provided a view of the entire enzyme in solution (the progress is reviewed by Spyroulias et al. (2004)). In addition, although normal-mode analysis work has suggested a mechanism by which the enzyme may open to allow in substrate or inhibitor (Watermeyer et al., 2006), the accessibility of the active site has not been systematically examined, and this may play a more important role than is yet understood.

Another useful direction to explore is the kinetic and structural characterisation of tACE-g13 active site mutants, particularly at the S1' and S2' sub-sites. This work is ongoing in our laboratory, and may bring some insight into the individual contributions of residues to the selectivity.

The modelling protocol has proved to be useful, although it is not yet optimal. After optimisation of the protocol the modelling and analysis of binding for other phosphinate inhibitors is also likely to suggest ways in which to enhance C-domain selectivity.

5. REFERENCES

List of References

Acharya KR, Sturrock ED, Riordan JF, Ehlers MR. 2003. Ace revisited: a new target for structure-based drug design. *Nat Rev Drug Discov 2*:891-902.

Alberts IL, Nadassy K, Wodak SJ. 1998. Analysis of zinc binding sites in protein crystal structures. *Protein Sci 7*:1700-1716.

Araujo MC, Melo RL, Cesari MH, Juliano MA, Juliano L, Carmona AK. 2000. Peptidase specificity characterization of C- and N-terminal catalytic sites of angiotensin I-converting enzyme. *Biochemistry 39*:8519-8525.

Arndt JW, Hao B, Ramakrishnan V, Cheng T, Chan SI, Chan MK. 2002. Crystal structure of a novel carboxypeptidase from the hyperthermophilic archaeon Pyrococcus furiosus. *Structure (Camb) 10*:215-224.

Azizi M, Rousseau A, Ezan E, Guyene TT, Michelet S, Grognet JM, Lenfant M, Corvol P, Menard J. 1996. Acute angiotensin-converting enzyme inhibition increases the plasma level of the natural stem cell regulator N-acetyl-seryl-aspartyl-lysyl-proline. *J Clin Invest 97*:839-844.

Baudin B. 2002. New aspects on angiotensin-converting enzyme: from gene to disease. *Clin Chem Lab Med 40*:256-265.

Baudin B, Alves N, Pilon A, Beneteau-Burnat B, Giboudeau J. 1997. Structural and biological roles of glycosylations in pulmonary angiotensin I-converting enzyme. *Glycobiology 7*:565-570.

Bersanetti PA, Andrade MC, Casarini DE, Juliano MA, Nchinda AT, Sturrock ED, Juliano L, Carmona AK. 2004. Positional-scanning combinatorial libraries of fluorescence resonance energy transfer peptides for defining substrate specificity of the angiotensin I-converting enzyme and development of selective C-domain substrates. *Biochemistry 43*:15729-15736.

Binevski PV, Sizova EA, Pozdnev VF, Kost OA. 2003. Evidence for the negative cooperativity of the two active sites within bovine somatic angiotensin-converting enzyme. *FEBS Lett 550*:84-88.

Binkowski TA, Naghibzadeh S, Liang J. 2003. CASTp: Computed Atlas of Surface Topography of proteins. *Nucleic Acids Res 31*:3352-3355.

Brew K. 2003. Structure of human ACE gives new insights into inhibitor binding and design. *Trends Pharmacol Sci 24*:391-394.

Brooks BR, Bruccoleri RE, Olafson BD, States DJ, Swaminathan S, Karplus M. 1983. CHARMM: A Program for Macromolecular Energy, Minimization, and Dynamics Calculations. *J Comput Chem 4*:187-217.

Brown CK, Madauss K, Lian W, Beck MR, Tolbert WD, Rodgers DW. 2001. Structure of neurolysin reveals a deep channel that limits substrate access. *Proc Natl Acad Sci U S A 98*:3127-3132.

Brunger AT, Adams PD, Clore GM, DeLano WL, Gros P, Grosse-Kunstleve RW, Jiang JS, Kuszewski J, Nilges M, Pannu NS, Read RJ, Rice LM, Simonson T, Warren GL. 1998. Crystallography & NMR system: A new software suite for macromolecular structure determination. *Acta Crystallogr D Biol Crystallogr 54*:905-921.

Bueno V, Palos M, Ronchi FA, Andrade MC, Ginoza M, Casarini DE. 2004. N-Domain angiotensin I-converting enzyme expression in renal artery of Wistar, Wistar Kyoto, and spontaneously hypertensive rats. *Transplant Proc 36*:1001-1003.

Bunning P, Holmquist B, Riordan JF. 1983. Substrate specificity and kinetic characteristics of angiotensin converting enzyme. *Biochemistry 22*:103-110.

Bunning P, Riordan JF. 1983. Activation of angiotensin converting enzyme by monovalent anions. *Biochemistry 22*:110-116.

Campbell DJ. 1987. Circulating and tissue angiotensin systems. *J Clin Invest 79*:1-6.

Casarini DE, Plavinik FL, Zanella MT, Marson O, Krieger JE, Hirata IY, Stella RC. 2001. Angiotensin converting enzymes from human urine of mild hypertensive untreated patients resemble the N-terminal fragment of human angiotensin I-converting enzyme. *Int J Biochem Cell Biol 33*:75-85.

Chen R, Li L, Weng Z. 2003. ZDOCK: an initial-stage protein-docking algorithm. *Proteins 52*:80-87.

Cheng TC, Ramakrishnan V, Chan SI. 1999. Purification and characterization of a cobalt-activated carboxypeptidase from the hyperthermophilic archaeon Pyrococcus furiosus. *Protein Sci 8*:2474-2486.

Chenna R, Sugawara H, Koike T, Lopez R, Gibson TJ, Higgins DG, Thompson JD. 2003. Multiple sequence alignment with the Clustal series of programs. *Nucleic Acids Res 31*:3497-3500.

Coates D, Isaac RE, Cotton J, Siviter R, Williams TA, Shirras A, Corvol P, Dive V. 2000. Functional conservation of the active sites of human and Drosophila angiotensin I-converting enzyme. *Biochemistry 39*:8963-8969.

Colman PM, Jansonius JN, Matthews BW. 1972. The structure of thermolysin: an electron density map at 2-3 A resolution. *J Mol Biol 70*:701-724.

Corradi HR, Schwager SL, Nchinda AT, Sturrock ED, Acharya KR. 2006. Crystal structure of the N domain of human somatic angiotensin I-converting enzyme provides a structural basis for domain-specific inhibitor design. *J Mol Biol 357*:964-974.

Crackower MA, Sarao R, Oudit GY, Yagil C, Kozieradzki I, Scanga SE, Oliveira-dos-Santos AJ, da Costa J, Zhang L, Pei Y, Scholey J, Ferrario CM, Manoukian AS, Chappell MC, Backx PH, Yagil Y, Penninger JM. 2002. Angiotensin-converting enzyme 2 is an essential regulator of heart function. *Nature 417*:822-828.

Cushman DW, Cheung HS, Sabo EF, Ondetti MA. 1977. Design of potent competitive inhibitors of angiotensin-converting enzyme. Carboxyalkanoyl and mercaptoalkanoyl amino acids. *Biochemistry 16*:5484-5491.

Cushman DW, Ondetti MA. 1980. Inhibitors of angiotensin-converting enzyme for treatment of hypertension. *Biochem Pharmacol 29*:1871-1877.

Cushman DW, Ondetti MA. 1999. Design of angiotensin converting enzyme inhibitors. *Nat Med 5*:1110-1113.

Danilczyk U, Eriksson U, Crackower MA, Penninger JM. 2003. A story of two ACEs. *J Mol Med 81*:227-234.

Danser AH, Saris JJ, Schuijt MP, van Kats JP. 1999. Is there a local renin-angiotensin system in the heart? *Cardiovasc Res 44*:252-265.

Davis IW, Murray LW, Richardson JS, Richardson DC. 2004. MOLPROBITY: structure validation and all-atom contact analysis for nucleic acids and their complexes. *Nucleic Acids Res 32*:W615-W619.

Deddish PA, Marcic B, Jackman HL, Wang HZ, Skidgel RA, Erdos EG. 1998. N-domain-specific substrate and C-domain inhibitors of angiotensin-converting enzyme: angiotensin-(1-7) and keto-ACE. *Hypertension 31*:912-917.

Deddish PA, Wang J, Michel B, Morris PW, Davidson NO, Skidgel RA, Erdos EG. 1994. Naturally occurring active N-domain of human angiotensin I-converting enzyme. *Proc Natl Acad Sci U S A 91*:7807-7811.

DeLano WL. 2002. The PyMOL Molecular Graphics System. DeLano Scientific, San Carlos CA, USA. http://www.pymol.org.

Dive V, Cotton J, Yiotakis A, Michaud A, Vassiliou S, Jiracek J, Vazeux G, Chauvet MT, Cuniasse P, Corvol P. 1999. RXP 407, a phosphinic peptide, is a potent inhibitor of angiotensin I converting enzyme able to differentiate between its two active sites. *Proc Natl Acad Sci U S A 96*:4330-4335.

Dive V, Georgiadis D, Matziari M, Makaritis A, Beau F, Cuniasse P, Yiotakis A. 2004. Phosphinic peptides as zinc metalloproteinase inhibitors. *Cell Mol Life Sci 61*:2010-2019.

Dzau VJ. 1988. Circulating versus local renin-angiotensin system in cardiovascular homeostasis. *Circulation 77*:I4-13.

Ehlers MR, Chen YN, Riordan JF. 1991a. Purification and characterization of recombinant human testis angiotensin-converting enzyme expressed in Chinese hamster ovary cells. *Protein Expr Purif 2*:1-9.

Ehlers MR, Chen YN, Riordan JF. 1992. The unique N-terminal sequence of testis angiotensin-converting enzyme is heavily O-glycosylated and unessential for activity or stability. *Biochem Biophys Res Commun 183*:199-205.

Ehlers MR, Riordan JF. 1989. Angiotensin-converting enzyme: new concepts concerning its biological role. *Biochemistry 28*:5311-5318.

Ehlers MR, Riordan JF. 1991. Angiotensin-converting enzyme: zinc- and inhibitor-binding stoichiometries of the somatic and testis isozymes. *Biochemistry 30*:7118-7126.

Ehlers MR, Schwager SL, Scholle RR, Manji GA, Brandt WF, Riordan JF. 1996. Proteolytic release of membrane-bound angiotensin-converting enzyme: role of the juxtamembrane stalk sequence. *Biochemistry 35*:9549-9559.

Ehlers MRW, Chen YN, Riordan JF. 1991b. Purification and characterization of recombinant human testis angiotensin-converting enzyme expressed in chinese hamster ovary cells. *Protein Expression and Purification 2*:1-9.

Erdos EG, Skidgel RA. 1987. The angiotensin I-converting enzyme. *Lab Invest 56*:345-348.

Erdos EG, Yang HY. 1967. An enzyme in microsomal fraction of kidney that inactivates bradykinin. *Life Sci 6*:569-574.

Eriksson U, Danilczyk U, Penninger JM. 2002. Just the beginning: novel functions for angiotensin-converting enzymes. *Curr Biol 12*:R745-R752.

Esther CR, Marino EM, Howard TE, Machaud A, Corvol P, Capecchi MR, Bernstein KE. 1997. The critical role of tissue angiotensin-converting enzyme as revealed by gene targeting in mice. *J Clin Invest 99*:2375-2385.

Fernandez JH, Hayashi MA, Camargo AC, Neshich G. 2003. Structural basis of the lisinopril-binding specificity in N- and C-domains of human somatic ACE. *Biochem Biophys Res Commun 308*:219-226.

Ferrario CM, Iyer SN. 1998. Angiotensin-(1-7): a bioactive fragment of the renin-angiotensin system. *Regulatory Peptides 78*:13-18.

Friedland J, Silverstein E. 1976. A sensitive fluorimetric assay for serum angiotensin-converting enzyme. *Am J Clin Pathol 66*:416-424.

Galanis AS, Spyroulias GA, Pierattelli R, Tzakos A, Troganis A, Gerothanassis IP, Pairas G, Manessi-Zoupa E, Cordopatis P. 2003. Zinc binding in peptide models of angiotensin-I converting enzyme active sites studied through 1H-NMR and chemical shift perturbation mapping. *Biopolymers 69*:244-252.

Gall AL, Ruff M, Kannan R, Cuniasse P, Yiotakis A, Dive V, Rio MC, Basset P, Moras D. 2001. Crystal structure of the stromelysin-3 (MMP-11) catalytic domain complexed with a phosphinic inhibitor mimicking the transition-state. *J Mol Biol 307*:577-586.

Georgiadis D, Beau F, Czarny B, Cotton J, Yiotakis A, Dive V. 2003. Roles of the two active sites of somatic angiotensin-converting enzyme in the cleavage of angiotensin I and bradykinin: insights from selective inhibitors. *Circ Res 93*:148-154.

Georgiadis D, Cuniasse P, Cotton J, Yiotakis A, Dive V. 2004. Structural determinants of RXPA380, a potent and highly selective inhibitor of the angiotensin-converting enzyme C-domain. *Biochemistry 43*:8048-8054.

Gewirth D, Majewski W. 2003. The SCALEPACK Manual, p. 88-96. In The HKL Manual.

Glaeser R, Facciotti M, Walian P, Rouhani S, Holton J, MacDowell A, Celestre R, Cambie D, Padmore H. 2000. Characterization of conditions required for X-Ray diffraction experiments with protein microcrystals. *Biophys J 78*:3178-3185.

Goodsell DS, Morris GM, Olson AJ. 1996. Automated docking of flexible ligands: applications of AutoDock. *J Mol Recognit 9*:1-5.

Gordon K, Redelinghuys P, Schwager SL, Ehlers MR, Papageorgiou AC, Natesh R, Acharya KR, Sturrock ED. 2003. Deglycosylation, processing and crystallization of human testis angiotensin-converting enzyme. *Biochem J 371*:437-442.

Hooper NM. 1994. Families of zinc metalloproteases. *FEBS Lett 354*:1-6.

Houard X, Williams TA, Michaud A, Dani P, Isaac RE, Shirras AD, Coates D, Corvol P. 1998. The Drosophila melanogaster-related angiotensin-I-converting enzymes Acer and Ance--distinct enzymic characteristics and alternative expression during pupal development. *Eur J Biochem 257*:599-606.

Hurst D, Rylett CM, Isaac RE, Shirras AD. 2003. The drosophila angiotensin-converting enzyme homologue Ance is required for spermiogenesis. *Dev Biol 254*:238-247.

Jaspard E, Wei L, Alhenc-Gelas F. 1993. Differences in the properties and enzymatic specificities of the two active sites of angiotensin I-converting enzyme (kininase II). Studies with bradykinin and other natural peptides. *J Biol Chem 268*:9496-9503.

Jones TA, Bergdoll M, Kjeldgaard M. 1990. O: A macromolecular modeling environment. In: Crystallographic and Modeling Methods in Molecular Design. Eds.: C. Bugg & S. Ealick. 189-195.

Junot C, Gonzales MF, Ezan E, Cotton J, Vazeux G, Michaud A, Azizi M, Vassiliou S, Yiotakis A, Corvol P, Dive V. 2001. RXP 407, a selective inhibitor of the N-domain of angiotensin I-converting enzyme, blocks in vivo the degradation of hemoregulatory peptide acetyl-Ser-Asp-Lys-Pro with no effect on angiotensin I hydrolysis. *J Pharmacol Exp Ther 297*:606-611.

Kasturi S, Jabbar MA, Sen GC, Sen I. 1994. Role of glycosylation in the biosynthesis and activity of rabbit testicular angiotensin-converting enzyme. *Biochemistry 33*:6228-6234.

Kim H, Lipscomb WN. 1990. Crystal structure of the complex of carboxypeptidase A with a strongly bound phosphonate in a new crystalline form: comparison with structures of other complexes. *Biochemistry 29*:5546-5555.

Kim HM, Shin DR, Yoo OJ, Lee H, Lee JO. 2003. Crystal structure of Drosophila angiotensin I-converting enzyme bound to captopril and lisinopril. *FEBS Lett 538*:65-70.

Kim J, Hewitt G, Carroll P, Sieburth SM. 2005. Silanediol inhibitors of angiotensin-converting enzyme. Synthesis and evaluation of four diastereomers of Phe[Si]Ala dipeptide analogues. *J Org Chem 70*:5781-5789.

Kim J, Sieburth SM. 2004. A silanediol inhibitor of the metalloprotease thermolysin: synthesis and comparison with a phosphinic acid inhibitor. *J Org Chem 69*:3008-3014.

Kissinger CR, Gehlhaar DK, Fogel DB. 1999. Rapid automated molecular replacement by evolutionary search. *Acta Crystallogr D Biol Crystallogr 55*:484-491.

Kleywegt GJ, Jones TA. 1996. xdlMAPMAN and xdlDATAMAN - programs for reformatting, analysis and manipulation of biomacromolecular electron-density maps and reflection data sets. *Acta Crystallogr D Biol Crystallogr 52*:826-828.

Kost OA, Bovin NV, Chemodanova EE, Nasonov VV, Orth TA. 2000. New feature of angiotensin-converting enzyme: carbohydrate-recognizing domain. *J Mol Recognit 13*:360-369.

Kost OA, Orth TA, Nikolskaya II, Nametkin SN, Levashov AV. 1998. Carbohydrates regulate the dimerization of angiotensin-converting enzyme. *Biochem Mol Biol Int 44*:535-542.

Kuster DJ, Marshall GR. 2005. Validated ligand mapping of ACE active site. *J Comput Aided Mol Des 19*:609-615.

Laskowski RA, MacArthur MW, Moss DS, Thornton JM. 1993. PROCHECK: a program to check the stereochemical quality of protein structures. *J Appl Cryst 26*:283-291.

Lipscomb WN. 1983. Structure and Catalysis of Enzymes. *Annual Review of Biochemistry 52*:17-34.

Marti-Renom MA, Stuart AC, Fiser A, Sanchez R, Melo F, Sali A. 2000. Comparative protein structure modeling of genes and genomes. *Annu Rev Biophys Biomol Struct 29:291-325.*:291-325.

Matthews BW. 1988. Structural Basis of the Action of Thermolysin and Related Zinc Peptidases. *Acc Chem Res 21*:333-340.

Mayer D, Naylor CB, Motoc I, Marshall GR. 1987. A unique geometry of the active site of angiotensin-converting enzyme consistent with structure-activity studies. *J Comput Aided Mol Des 1*:3-16.

Natesh R, Schwager SL, Evans HR, Sturrock ED, Acharya KR. 2004. Structural details on the binding of antihypertensive drugs captopril and enalaprilat to human testicular angiotensin I-converting enzyme. *Biochemistry 43*:8718-8724.

Natesh R, Schwager SL, Sturrock ED, Acharya KR. 2003. Crystal structure of the human angiotensin-converting enzyme-lisinopril complex. *Nature 421*:551-554.

Nchinda AT, Chibale K, Redelinghuys P, Sturrock ED. 2006a. Synthesis and molecular modeling of a lisinopril-tryptophan analogue inhibitor of angiotensin I-converting enzyme. *Bioorg Med Chem Lett 16(17)*:4616-4619.

Nchinda AT, Chibale K, Redelinghuys P, Sturrock ED. 2006b. Synthesis of novel keto-ACE analogues as domain-selective angiotensin I-converting enzyme inhibitors. *Bioorg Med Chem Lett 16(17)*:4612-4615.

Oefner C, Arcy A, Hennig M, Winkler FK, Dale GE. 2000. Structure of human neutral endopeptidase (neprilysin) complexed with phosphoramidon. *Journal of Molecular Biology 296*:341-349.

Ondetti MA, Rubin B, Cushman DW. 1977. Design of specific inhibitors of angiotensin-converting enzyme: new class of orally active antihypertensive agents. *Science 196*:441-444.

Otwinowski Z, Minor W. 1997. Processing of X-ray Diffraction Data Collected in Oscillation Mode. *Methods Enzymol 276*:307-326.

Oudit GY, Crackower MA, Backx PH, Penninger JM. 2003. The role of ACE2 in cardiovascular physiology. *Trends Cardiovasc Med 13*:93-101.

Patchett AA, Harris E, Tristram EW, Wyvratt MJ, Wu MT, Taub D, Peterson ER, Ikeler TJ, ten Broeke J, Payne LG, Ondeyka DL, Thorsett ED, Greenlee WJ, Lohr NS, Hoffsommer RD, Joshua H, Ruyle WV, Rothrock JW, Aster SD, Maycock AL, Robinson FM, Hirschmann R, Sweet CS, Ulm EH, Gross DM, Vassil TC, Stone CA. 1980. A new class of angiotensin-converting enzyme inhibitors. *Nature 288*:280-283.

Redelinghuys P, Nchinda AT, Sturrock ED. 2005. Development of domain-selective Angiotensin I-converting enzyme inhibitors. *Ann N Y Acad Sci 1056*:160-175.

Rhaleb NE, Peng H, Harding P, Tayeh M, LaPointe MC, Carretero OA. 2001. Effect of N-acetyl-seryl-aspartyl-lysyl-proline on DNA and collagen synthesis in rat cardiac fibroblasts. *Hypertension 37*:827-832.

Riordan JF. 2003. Angiotensin-I-converting enzyme and its relatives. *Genome Biol 4*:225.

Ronin C, Granier C, Caseti C, Bouchilloux S, Van Rietschoten J. 1981. Synthetic substrates for thyroid oligosaccharide transferase. Effects of peptide chain length and modifications in the Asn-Xaa-Thr-region. *Eur J Biochem 118*:159-164.

Soubrier F, Wei L, Hubert C, Clauser E, Alhenc-Gelas F, Corvol P. 1993. Molecular biology of the angiotensin I converting enzyme: II. Structure-function. Gene polymorphism and clinical implications. *J Hypertens 11*:599-604.

Spyroulias GA, Galanis AS, Pairas G, Manessi-Zoupa E, Cordopatis P. 2004. Structural features of angiotensin-I converting enzyme catalytic sites: conformational studies in solution, homology models and comparison with other zinc metallopeptidases. *Curr Top Med Chem 4*:403-429.

Strater N, Lipscomb WN. 1995. Transition state analogue L-leucinephosphonic acid bound to bovine lens leucine aminopeptidase: X-ray structure at 1.65 A resolution in a new crystal form. *Biochemistry 34*:9200-9210.

Sturrock ED, Natesh R, van Rooyen JM, Acharya KR. 2004. Structure of angiotensin I-converting enzyme. *Cell Mol Life Sci 61*:2677-2686.

Tatei K, Cai H, Ip YT, Levine M. 1995. Race: a Drosophila homologue of the angiotensin converting enzyme. *Mech Dev 51*:157-168.

Thunnissen MMGM, Andersson B, Samuelsson B, Wong CH, Haeggstrom JZ. 2002. Crystal structures of leukotriene A4 hydrolase in complex with captopril and two competitive tight-binding inhibitors. *FASEB J 16*:1648-1650.

Tipnis SR, Hooper NM, Hyde R, Karran E, Christie G, Turner AJ. 2000. A human homolog of angiotensin-converting enzyme. Cloning and functional expression as a captopril-insensitive carboxypeptidase. *J Biol Chem 275*:33238-33243.

Towler P, Staker B, Prasad SG, Menon S, Tang J, Parsons T, Ryan D, Fisher M, Williams D, Dales NA, Patane MA, Pantoliano MW. 2004. ACE2 X-ray structures reveal a large hinge-bending motion important for inhibitor binding and catalysis. *J Biol Chem 279*:17996-18007.

Turbanti L, Cerbai G, Di Bugno C, Giorgi R, Garzelli G, Criscuoli M, Renzetti AR, Subissi A, Bramanti G, DePriest SA. 1993. 1,2-Cyclomethylenecarboxylic monoamide hydroxamic derivatives. A novel class of non-amino acid angiotensin converting enzyme inhibitors. *J Med Chem 36*:699-707.

Turner AJ, Hooper NM. 2002. The angiotensin-converting enzyme gene family: genomics and pharmacology. *Trends Pharmacol Sci 23*:177-183.

Tzakos AG, Galanis AS, Spyroulias GA, Cordopatis P, Manessi-Zoupa E, Gerothanassis IP. 2003. Structure-function discrimination of the N- and C-catalytic domains of human angiotensin-converting enzyme: implications for Cl- activation and peptide hydrolysis mechanisms. *Protein Eng 16*:993-1003.

[illegible], Gerothanassis IP. 2003. Domain-selective ligand-binding modes and atomic level pharmacophore refinement in angiotensin I converting enzyme (ACE) inhibitors. *Chembiochem* 6:1089-1103.

Watermeyer JM. 2004. Human testis angiotensin-converting enzyme: Crystal structure of a glycosylation mutant and investigation of a putative hinge mechanism by normal mode analysis. *M.Sc. thesis*. University of Western Cape, South Africa.

Watermeyer JM, Sewell BT, Schwager S, Natesh R, Corradi HR, Acharya KR, Sturrock ED. 2006. Structure of testis ACE glycosylation mutants and evidence for conserved domain movement. *Biochemistry 45*:12654-12663.

Wei L, Alhenc-Gelas F, Corvol P, Clauser E. 1991. The two homologous domains of human angiotensin I-converting enzyme are both catalytically active. *J Biol Chem 266*:9002-9008.

Wei L, Clauser E, Alhenc-Gelas F, Corvol P. 1992. The two homologous domains of human angiotensin I-converting enzyme interact differently with competitive inhibitors. *J Biol Chem 267*:13398-13405.

Williams TA, Corvol P, Soubrier F, Clauser E. 1994. A recombinant form of angiotensin converting enzyme expressed from baculovirus-infected insect cells. *Biochimie 76*:312-314.

Williams TA, Michaud A, Houard X, Chauvet MT, Soubrier F, Corvol P. 1996. Drosophila melanogaster angiotensin I-converting enzyme expressed in Pichia pastoris resembles the C domain of the mammalian homologue and does not require glycosylation for secretion and enzymic activity. *Biochem J 318 (Pt 1)*:125-131.

Woodman ZL, Oppong SY, Cook S, Hooper NM, Schwager SL, Brandt WF, Ehlers MR, Sturrock ED. 2000. Shedding of somatic angiotensin-converting enzyme (ACE) is inefficient compared with testis ACE despite cleavage at identical stalk sites. *Biochem J 347 Pt 3*:711-718.

Yiotakis A, Lecoq A, Nicolaou A, Labadie J, Dive V. 1994. Phosphinic peptide analogues as potent inhibitors of Corynebacterium rathayii bacterial collagenase. *Biochem J 303 (Pt 1)*:323-327.

Yu XC, Sturrock ED, Wu Z, Biemann K, Ehlers MR, Riordan JF. 1997. Identification of N-linked glycosylation sites in human testis angiotensin-converting enzyme and expression of an active deglycosylated form. *J Biol Chem 272*:3511-3519.

Zaman MA, Oparil S, Calhoun DA. 2002. Drugs targeting the renin-angiotensin-aldosterone system. *Nat Rev Drug Discov 1*:621-636.

AMDG